Chapter 2

Photonic bandstructure calculations

2.1 Approximation of Maxwell eigenvalues and eigenfunctions

by Willy Dörfler

2.1.1 The Maxwell eigenvalue problem

We recall that for the time-harmonic case with frequency ω we derived for the spatially varying part of the electric field $\boldsymbol{x} \mapsto \boldsymbol{E}(\boldsymbol{x})$ the equation (1.17),

$$\boldsymbol{\nabla} \times \Big(\frac{1}{\mu}\boldsymbol{\nabla} \times \boldsymbol{E}\Big) = \omega^2 \varepsilon \boldsymbol{E}$$

with the additional constraint

$$\boldsymbol{\nabla} \cdot \big(\varepsilon \boldsymbol{E}\big) = 0.$$

For the material parameters we set $\mu = \mu_0 \mu_{\mathrm{r}}$ and $\varepsilon = \varepsilon_0 \varepsilon_{\mathrm{r}}$. Moreover, we assume here that Ω is bounded in $\mathbb{R}^3$ and we impose the boundary condition (1.20), $\boldsymbol{n} \times \boldsymbol{u} = \boldsymbol{0}$, of a perfect conductor on $\partial\Omega$. With the definitions $\lambda := (\omega/c)^2$ (c the speed of light, Section 1.1.4) and $\boldsymbol{u} := \boldsymbol{E}$ the eigenvalue problem now reads

$$\begin{aligned} \boldsymbol{\nabla} \times \Big(\frac{1}{\mu_{\mathrm{r}}}\boldsymbol{\nabla} \times \boldsymbol{u}\Big) &= \lambda \varepsilon_{\mathrm{r}} \boldsymbol{u} && \text{in } \Omega, \\ \boldsymbol{\nabla} \cdot \big(\varepsilon_{\mathrm{r}} \boldsymbol{u}\big) &= 0 && \text{in } \Omega, \\ \boldsymbol{n} \times \boldsymbol{u} &= \boldsymbol{0} && \text{on } \partial\Omega. \end{aligned}$$

W. Dörfler et al., *Photonic Crystals: Mathematical Analysis and Numerical Approximation*, Oberwolfach Seminars 42, DOI 10.1007/978-3-0348-0113-3_2, © Springer Basel AG 2011

λ is called Maxwell eigenvalue. Note that the problem for $\boldsymbol{u} := \boldsymbol{H}$ would lead to equations with ε_r and μ_r interchanged and the boundary condition $\boldsymbol{n} \cdot \boldsymbol{u} = 0$ (1.20). We will continue with the first version and the additional setting $\mu_\mathrm{r} = 1$, which is a reasonable choice for many applications.

The eigenvalue problem will be connected to the following problem, the (strong) *curl–curl source problem*: Let a (suitable) vector field $\boldsymbol{f}$ be given. Assume that we can define $\boldsymbol{u} := \boldsymbol{T}\boldsymbol{f}$ as the unique solution to the problem

$$\begin{aligned} \boldsymbol{\nabla} \times \boldsymbol{\nabla} \times \boldsymbol{u} &= \varepsilon_\mathrm{r} \boldsymbol{f} && \text{in } \Omega, \\ \boldsymbol{\nabla} \cdot \big(\varepsilon_\mathrm{r} \boldsymbol{u}\big) &= 0 && \text{in } \Omega, \\ \boldsymbol{n} \times \boldsymbol{u} &= \boldsymbol{0} && \text{on } \partial\Omega. \end{aligned} \tag{2.1}$$

This defines a linear operator $\boldsymbol{T}$. The connection to the eigenvalue problem is that we now seek a nontrivial $\boldsymbol{u}$ such that $\boldsymbol{u} = \boldsymbol{T}(\lambda \boldsymbol{u})$ or $\boldsymbol{T}\boldsymbol{u} = \boldsymbol{u}/\lambda$ (for $\lambda \neq 0$). Thus we have to study the spectrum of $\boldsymbol{T}$. The same can be done in the discrete case. This will be the guideline for the following section.

We restrict the considerations to the following classes of domains Ω and coefficients $\varepsilon_\mathrm{r}, \mu_\mathrm{r}$.

Assumption 2.1.1.

(1) Let $\Omega \subset \mathbb{R}^3$ be a bounded domain with a polygonal simply connected boundary.

(2) Let $\varepsilon_\mathrm{r} : \Omega \to \mathbb{R}$ be piecewise constant with two-sided bounds $1 \leq \varepsilon_\mathrm{r} \leq \varepsilon_\infty$ for some $\varepsilon_\infty \geq 1$, $\mu_\mathrm{r} = 1$.

For more general conditions on ε_r and μ_r, such as $\varepsilon_\mathrm{r}, \mu_\mathrm{r} \in \mathbb{C}$ or $\varepsilon_\mathrm{r}, \mu_\mathrm{r} \in \mathbb{R}^{3,3}$, and the related different techniques, see [19] [26, Ch. 4.2, 4.6].

2.1.2 The weak curl–curl source problem

The second equation in (2.1) is interpreted as a linear constraint on the first equation. We choose a *Lagrange 'parameter' p*, multiply the first equation by an arbitrary $\boldsymbol{v} \in H_0(\mathrm{curl}, \Omega)$ and the second with arbitrary $q \in H_0^1(\Omega)$ and integrate by parts to get the *weak curl–curl source problem*

$$\begin{aligned} \int_\Omega \big\{ \boldsymbol{\nabla} \times \boldsymbol{u} \cdot \boldsymbol{\nabla} \times \boldsymbol{v} + \varepsilon_\mathrm{r} \boldsymbol{\nabla} p \cdot \boldsymbol{v} \big\} &= \int_\Omega \varepsilon_\mathrm{r} \boldsymbol{f} \cdot \boldsymbol{v} && \text{for all } \boldsymbol{v} \in H_0(\mathrm{curl}, \Omega), \\ \int_\Omega \varepsilon_\mathrm{r} \boldsymbol{\nabla} q \cdot \boldsymbol{u} &= 0 && \text{for all } q \in H_0^1(\Omega). \end{aligned} \tag{2.2}$$

In the following we will use the abbreviations

$$\begin{aligned} \boldsymbol{V} &:= H_0(\mathrm{curl}, \Omega) \text{ with } \|\boldsymbol{v}\|_{\boldsymbol{V}} := \|\boldsymbol{v}\|_{H(\mathrm{curl}, \Omega)}, \\ Q &:= H_0^1(\Omega) \text{ with } \|q\|_Q := \|\boldsymbol{\nabla} q\|_{L^2(\Omega)^3}. \end{aligned}$$

Note that due to Assumption 2.1.1.(2), we have $\boldsymbol{f} \in L^2(\Omega)^3$ if and only if $\varepsilon_{\mathrm{r}}\boldsymbol{f} \in L^2(\Omega)^3$. The above problem is then formalised as to find $\boldsymbol{u} \in \boldsymbol{V}$ and $p \in Q$ with

$$\begin{aligned} a(\boldsymbol{u},\boldsymbol{v}) + b(p,\boldsymbol{v}) &= F(\boldsymbol{v}) \qquad \text{for all } \boldsymbol{v} \in \boldsymbol{V}, \\ b(q,\boldsymbol{u}) &= 0 \qquad \text{for all } q \in Q, \end{aligned} \tag{2.3}$$

with continuous bilinear forms, resp., linear form

$$a : \boldsymbol{V} \times \boldsymbol{V} \to \mathbb{R}, \quad a(\boldsymbol{w},\boldsymbol{v}) := \int_\Omega \boldsymbol{\nabla} \times \boldsymbol{w} \cdot \boldsymbol{\nabla} \times \boldsymbol{v}, \tag{2.4}$$

$$b : Q \times \boldsymbol{V} \to \mathbb{R}, \quad b(q,\boldsymbol{v}) := \int_\Omega \varepsilon_{\mathrm{r}} \boldsymbol{\nabla} q \cdot \boldsymbol{v}, \tag{2.5}$$

$$F : \boldsymbol{V} \to \mathbb{R}, \quad F(\boldsymbol{v}) := \int_\Omega \varepsilon_{\mathrm{r}} \boldsymbol{f} \cdot \boldsymbol{v}. \tag{2.6}$$

Reduction to a single equation

We incorporate the constraint into the space and therefore seek $\boldsymbol{u} \in \boldsymbol{V}_{\varepsilon_{\mathrm{r}}}$ with

$$\boldsymbol{V}_{\varepsilon_{\mathrm{r}}} := \big\{ \boldsymbol{v} \in \boldsymbol{V} \,:\, b(q,\boldsymbol{v}) = 0 \text{ for all } q \in Q \big\}. \tag{2.7}$$

Then the second equation is automatically satisfied and it remains

$$a(\boldsymbol{u},\boldsymbol{v}) = F(\boldsymbol{v}) \qquad \text{for all } \boldsymbol{v} \in \boldsymbol{V}_{\varepsilon_{\mathrm{r}}}. \tag{2.8}$$

Existence

([23] [19, Ch. 4] [26, Ch. 3.4]). Existence and uniqueness for these type of equations will be proved via the Babuška–Brezzi Theorem 1.2.6. In order to establish the requirements, Theorem 1.2.1 would be the right tool for the following arguments if ε_{r} would be constant. But we now need requirements on $\boldsymbol{\nabla}\cdot(\varepsilon_{\mathrm{r}}\boldsymbol{u})$ instead of $\boldsymbol{\nabla}\cdot\boldsymbol{u}$. However, the result can be reformulated correspondingly.

Theorem 2.1.2. *Let $\Omega \subset \mathbb{R}^3$ and ε_{r} as in Assumption* 2.1.1. *Then the space $X_{\mathrm{N}}(\Omega;\varepsilon_{\mathrm{r}}) := H_0(\mathrm{curl},\Omega) \cap H(\mathrm{div}(\varepsilon_{\mathrm{r}}\,.\,),\Omega)$ is continuously embedded in $H^s(\Omega)^3$ for some $s > 0$, more precisely, for each of its elements holds*

$$\|\boldsymbol{v}\|_{H^s(\Omega)^3} \le C\big(\|\boldsymbol{v}\|_{\boldsymbol{V}} + \|\boldsymbol{\nabla}\cdot(\varepsilon_{\mathrm{r}}\boldsymbol{v})\|_{L^2(\Omega)^3}\big)$$

with $C > 0$, depending on $\Omega, \varepsilon_{\mathrm{r}}, s$. Especially, $\boldsymbol{V}_{\varepsilon_{\mathrm{r}}}$ is compactly embedded in $L^2(\Omega)^3$. If ε_{r} is uniformly Lipschitz-continuous, then one can find $s > 1/2$. If, in addition to that, Ω is convex, then we can take $s = 1$. A corresponding result holds for $\boldsymbol{v} \in X_{\mathrm{T}}(\Omega;\varepsilon_{\mathrm{r}}) := H(\mathrm{curl},\Omega) \cap H_0(\mathrm{div}(\varepsilon_{\mathrm{r}}\,.\,),\Omega)$.

Proof. [19, Thm. 4.1, Lem. 4.2, Cor. 4.3]. Let $\boldsymbol{v} \in X_{\mathrm{N}}(\Omega;\varepsilon_{\mathrm{r}})$. Application of the Regular decomposition Theorem 1.2.4, that actually holds also under the stated requirement on $\boldsymbol{v}$, establishes $\boldsymbol{v} = \boldsymbol{z} + \boldsymbol{\nabla} q$ for $\boldsymbol{z} \in H^1(\Omega)^3$ and $q \in Q$. Multiplying

by ε_{r} and taking (formally) the divergence yields the boundary value problem $-\boldsymbol{\nabla}\cdot(\varepsilon_{\mathrm{r}}\boldsymbol{\nabla}q) = \boldsymbol{\nabla}\cdot(\varepsilon_{\mathrm{r}}\boldsymbol{z}) - \boldsymbol{\nabla}\cdot(\varepsilon_{\mathrm{r}}\boldsymbol{v})$ in Ω, $q = 0$ on $\partial\Omega$, to be interpreted in the weak sense. While the second term on the right is in $L^2(\Omega)^3$ by assumption, the first term will be in $L^2(\Omega)^3$ only if ε_{r} is sufficiently regular (e. g., uniformly Lipschitz), but a distribution otherwise. The result follows from the elaborated regularity theory for elliptic equations with Dirichlet boundary condition that results in the bound $\|\boldsymbol{\nabla}q\|_{H^s(\Omega)^3} \leq C(\|\boldsymbol{z}\|_{H^1(\Omega)^3} + \|\boldsymbol{\nabla}\cdot(\varepsilon_{\mathrm{r}}\boldsymbol{v})\|_{L^2(\Omega)^3})$ which leads immediately to the stated bound [14]. We note, that for $\boldsymbol{v} \in \boldsymbol{V}_{\varepsilon_{\mathrm{r}}}$ we get the bound $\|\boldsymbol{v}\|_{H^s(\Omega)^3} \leq C\|\boldsymbol{v}\|_{\boldsymbol{V}}$ which proves the compactness.

For the case of $X_{\mathrm{T}}(\Omega;\varepsilon_{\mathrm{r}})$ we have $\boldsymbol{n}\cdot\boldsymbol{\nabla}q = 0$ as a boundary condition and can refer to regularity results for the homogeneous Neumann problem [14]. □

Theorem 2.1.3 (Poincaré–Friedrich–type inequality). *Let $\Omega \subset \mathbb{R}^3$ and ε_{r} as in Assumption* 2.1.1*. Then*

$$\|\boldsymbol{v}\|_{L^2(\Omega)^3} \leq C_{\mathrm{F}}\|\boldsymbol{\nabla}\times\boldsymbol{v}\|_{L^2(\Omega)^3} \tag{2.9}$$

holds for all $\boldsymbol{v} \in \boldsymbol{V}_{\varepsilon_{\mathrm{r}}}$ with a constant $C_{\mathrm{F}} > 0$.

Proof. The proof is indirect: Assuming that the assertion is wrong, we have a sequence $\{\boldsymbol{v}_n\}_{n\in\mathbb{N}} \subset \boldsymbol{V}_{\varepsilon_{\mathrm{r}}}$ that satisfies $\|\boldsymbol{v}_n\|_{L^2(\Omega)^3} = 1$ and $\|\boldsymbol{\nabla}\times\boldsymbol{v}_n\|_{L^2(\Omega)^3} \to 0$. Using the compact embedding into $L^2(\Omega)^3$, Theorem 2.1.2, we find a limit $\boldsymbol{v}$ of a subsequence that satisfies: $\|\boldsymbol{v}\|_{L^2(\Omega)^3} = 1$ and $\|\boldsymbol{\nabla}\times\boldsymbol{v}\|_{L^2(\Omega)^3} = 0$. By Theorem 1.2.2 we see that $\boldsymbol{v} = \boldsymbol{\nabla}p$ for some $p \in H^1(\Omega)$. Since $\boldsymbol{n}\times\boldsymbol{v} = \boldsymbol{n}\times\boldsymbol{\nabla}p = \boldsymbol{0}$ on $\partial\Omega$, p is constant on $\partial\Omega$ and we can choose $p = 0$ on $\partial\Omega$. Now p fulfills $\boldsymbol{\nabla}\cdot(\varepsilon_{\mathrm{r}}\boldsymbol{\nabla}p) = 0$ (in the weak sense) with homogeneous boundary conditions and thus $p = 0$ and so $\boldsymbol{v} = \boldsymbol{0}$. This however contradicts $\|\boldsymbol{v}\|_{L^2(\Omega)^3} = 1$ [26, Cor. 3.51, Cor. 4.8]. □

Theorem 2.1.4. *Let $\Omega \subset \mathbb{R}^3$ and ε_{r} as in Assumption* 2.1.1*. Then, for any given $\boldsymbol{f} \in L^2(\Omega)^3$, there is a unique solution $[\boldsymbol{u}, p] \in \boldsymbol{V}_{\varepsilon_{\mathrm{r}}} \times Q$ to the weak curl–curl source problem* (2.2) *and it satisfies the a priori bound*

$$\|\boldsymbol{u}\|_{\boldsymbol{V}} + \|p\|_Q \leq C\|\boldsymbol{f}\|_{L^2(\Omega)^3}$$

for $C := (C_{\mathrm{F}}^2 + 2)\varepsilon_\infty$.

Proof. We take a, b, F from (2.5)–(2.6) and identify $H := \boldsymbol{V}$, $K := \boldsymbol{V}_{\varepsilon_{\mathrm{r}}}$, and $M := Q$. From Theorem 2.1.3 we obtain the bound

$$\|\boldsymbol{v}\|_{L^2(\Omega)^3} \leq C_{\mathrm{F}}\|\boldsymbol{\nabla}\times\boldsymbol{v}\|_{L^2(\Omega)^3} \qquad \text{for all } \boldsymbol{v} \in \boldsymbol{V}_{\varepsilon_{\mathrm{r}}}.$$

Then we have coercivity of the bilinear form a on $\boldsymbol{V}_{\varepsilon_{\mathrm{r}}}$, since then

$$\begin{aligned} a(\boldsymbol{v},\boldsymbol{v}) = \|\boldsymbol{\nabla}\times\boldsymbol{v}\|^2_{L^2(\Omega)^3} &= \frac{C_{\mathrm{F}}^2}{C_{\mathrm{F}}^2+1}\|\boldsymbol{\nabla}\times\boldsymbol{v}\|^2_{L^2(\Omega)^3} + \frac{1}{C_{\mathrm{F}}^2+1}\|\boldsymbol{\nabla}\times\boldsymbol{v}\|^2_{L^2(\Omega)^3} \\ &\geq \frac{1}{C_{\mathrm{F}}^2+1}\Big(\|\boldsymbol{v}\|^2_{L^2(\Omega)^3} + \|\boldsymbol{\nabla}\times\boldsymbol{v}\|^2_{L^2(\Omega)^3}\Big) = \frac{1}{C_{\mathrm{F}}^2+1}\|\boldsymbol{v}\|^2_{\boldsymbol{V}}. \end{aligned}$$

To prove the inf–sup–condition choose an arbitrary smooth $q \in Q$ and let $\boldsymbol{v}_q := \boldsymbol{\nabla} q \in L^2(\Omega)^3$. With $\boldsymbol{\nabla} \times \boldsymbol{\nabla} q = \boldsymbol{0}$ we see that $\boldsymbol{v}_q \in H(\mathrm{curl}, \Omega)$. Since $q\big|_{\partial\Omega} = 0$ we have that $\boldsymbol{\nabla} q\big|_{\partial\Omega}$ is proportional to the normal vector $\boldsymbol{n}$ to $\partial\Omega$ and thus $\boldsymbol{n} \times \boldsymbol{\nabla} q = \boldsymbol{0}$, hence $\boldsymbol{v}_q \in \boldsymbol{V}$. Thus it holds

$$\sup_{\boldsymbol{v} \in \boldsymbol{V} \setminus \{\boldsymbol{0}\}} \frac{b(q, \boldsymbol{v})}{\|v\|_{\boldsymbol{V}}} \geq \frac{b(q, \boldsymbol{v}_q)}{\|\boldsymbol{v}_q\|_{\boldsymbol{V}}} \geq \min_{\boldsymbol{x} \in \Omega} \{\varepsilon_{\mathrm{r}}(\boldsymbol{x})\} \frac{\|\boldsymbol{\nabla} q\|^2_{L^2(\Omega)^3}}{\|\boldsymbol{\nabla} q\|_{L^2(\Omega)^3}} \geq \|q\|_Q$$

and the inf–sup–condition follows readily from this. Note, that the proof relies on the property $\boldsymbol{\nabla} Q \subset \boldsymbol{V}$. The continuity of the right hand side in (2.8) is easily verified by

$$\begin{aligned} |F(\boldsymbol{v})| &= \Big| \int_\Omega \varepsilon_{\mathrm{r}} \boldsymbol{f} \cdot \boldsymbol{v} \Big| \leq \|\varepsilon_{\mathrm{r}} \boldsymbol{f}\|_{L^2(\Omega)^3} \, \|\boldsymbol{v}\|_{L^2(\Omega)^3} \\ &\leq \varepsilon_\infty \|\boldsymbol{f}\|_{L^2(\Omega)^3} \, \|\boldsymbol{v}\|_{\boldsymbol{V}} \end{aligned}$$

for all $\boldsymbol{v} \in \boldsymbol{V}$. Applying Theorem 1.2.6 proves existence and uniqueness. The estimate follows immediately from (2.8) and the given bounds on a and F. □

Theorem 2.1.5. *Let $\Omega \subset \mathbb{R}^3$ and ε_{r} as in Assumption* 2.1.1*. Then the mapping $\boldsymbol{T} : L^2(\Omega)^3 \to \boldsymbol{V}_{\varepsilon_{\mathrm{r}}} \subset L^2(\Omega)^3$, $\boldsymbol{f} \mapsto \boldsymbol{T}\boldsymbol{f} := \boldsymbol{u}$, with $\boldsymbol{u}$ from Theorem* 2.1.4*, is linear and continuous. Moreover, $\boldsymbol{u} \in H^s(\Omega)^3$ for some $s > 0$ and hence $\boldsymbol{T}$ is compact.*

Proof. The first assertion is a direct consequence of the previous Theorem 2.1.4. The regularity of $\boldsymbol{u}$ and the compactness of $\boldsymbol{T}$ follows from Theorem 2.1.2. □

Remark 2.1.6. In case $\boldsymbol{f} \in \boldsymbol{V}_{\varepsilon_{\mathrm{r}}}$ we find $p = 0$. Indeed, taking $\boldsymbol{v} := \boldsymbol{\nabla} q \in \boldsymbol{V}$ for $q \in Q$ as a test function, we obtain the weak formulation for $-\boldsymbol{\nabla} \cdot (\varepsilon_{\mathrm{r}} \boldsymbol{\nabla} p) = 0$ in Ω, $p = 0$ on $\partial\Omega$, which is uniquely solved by $p = 0$. However, if $\boldsymbol{f} \notin \boldsymbol{V}_{\varepsilon_{\mathrm{r}}}$, then $p \not\equiv 0$ and thus $\boldsymbol{u}$ is not a weak solution of (2.1) but

$$\begin{aligned} \boldsymbol{\nabla} \times \boldsymbol{\nabla} \times \boldsymbol{u} + \varepsilon_{\mathrm{r}} \boldsymbol{\nabla} p &= \varepsilon_{\mathrm{r}} \boldsymbol{f} && \text{in } \Omega, \\ \boldsymbol{\nabla} \cdot \big(\varepsilon_{\mathrm{r}} \boldsymbol{u}\big) &= 0 && \text{in } \Omega, \\ \boldsymbol{n} \times \boldsymbol{u} &= \boldsymbol{0} && \text{on } \partial\Omega. \end{aligned} \tag{2.10}$$

Thus, (2.10) is the correct definition for $\boldsymbol{T}\boldsymbol{f}$ in the strong form.

Theorem 2.1.7. *Let $\Omega \subset \mathbb{R}^3$ and ε_{r} as in Assumption 2.1.1. Then there exists a discrete set of positive Maxwell eigenvalues with eigenspaces of finite multiplicity.*

Proof. The weak form of the eigenvalue problem is given by (2.2) with $\boldsymbol{f}$ replaced by $\lambda \boldsymbol{u}$. Taking $\boldsymbol{v} = \boldsymbol{u}$ we see that all eigenvalues are a priori non-negative. Note that according to Remark 2.1.6 we will find $p = 0$. Since the weak curl–curl problem is uniquely solvable, there is no zero eigenvalue. Thus all Maxwell eigenvalues are eigenvalues of $\boldsymbol{T}$, since $\boldsymbol{T}\boldsymbol{u} = 1/\lambda \, \boldsymbol{u}$. The assertion for $\boldsymbol{T}$ follows from its compactness (Theorem 2.1.5). □

2.1.3 The discrete curl–curl source problem

We choose a *Galerkin method* to find a numerical approximation to (2.1) in that we formulate (2.2) in terms of discrete spaces $\boldsymbol{V}^h \subset \boldsymbol{V}$ and $Q_h \subset Q$ with inherited norms. Usually, these spaces are defined to be piecewise polynomial functions on a decomposition of Ω into a collection of "elements" like tetrahedra or hexahedra. The regularity of these functions at the interfaces has to be such that the trace operators are well defined. The parameter h symbolises the maximal diameter of such elements and it will be the quantity that we refer to in the error estimates which study the behaviour for $h \to 0$. We will here not consider the influence of an approximation of Ω ($\Omega = \Omega_h$) and the permittivity ε_{r} ($\varepsilon_{\mathrm{r}} = \varepsilon_{\mathrm{r},h}$). Thus we seek $\boldsymbol{u}^h \in \boldsymbol{V}^h$, $p_h \in Q_h$ such that, with a, b, F as in (2.4)–(2.4)

$$\begin{aligned} a(\boldsymbol{u}^h, \boldsymbol{v}^h) + b(\boldsymbol{v}^h, p_h) &= F(\boldsymbol{v}^h) \qquad \text{for all } \boldsymbol{v}^h \in \boldsymbol{V}^h, \\ b(\boldsymbol{u}^h, q_h) &= 0 \qquad \text{for all } q_h \in Q_h. \end{aligned} \tag{2.11}$$

Again, as in Section 2.1.2, we can reduce this system to one equation on a constraint space. Let

$$\boldsymbol{V}^h_{\varepsilon_{\mathrm{r}}} := \left\{ \boldsymbol{w}^h \in \boldsymbol{V}^h \,:\, b(q_h, \boldsymbol{w}^h) = 0 \text{ for all } q_h \in Q_h \right\}$$

and seek $\boldsymbol{u}^h \in \boldsymbol{V}^h_{\varepsilon_{\mathrm{r}}}$ such that

$$a(\boldsymbol{u}^h, \boldsymbol{v}^h) = F(\boldsymbol{v}^h) \qquad \text{for all } \boldsymbol{v}^h \in \boldsymbol{V}^h_{\varepsilon_{\mathrm{r}}}.$$

The discrete problem is again of the type (2.3) and existence und uniqueness requires the validity of the conditions in Theorem 1.2.6. By Theorem 2.1.4 the requirements can be stated as follows.

Theorem 2.1.8. *Assume that an estimate like* (2.9) *holds with constant* C_{dF} *for all* $\boldsymbol{v}^h \in \boldsymbol{V}^h_{\varepsilon_{\mathrm{r}}}$ *and that* $\boldsymbol{\nabla} Q_h \subset \boldsymbol{V}^h$. *For any given* $\boldsymbol{f} \in L^2(\Omega)^3$, *there is a unique solution* $\boldsymbol{u}^h \in \boldsymbol{V}^h_{\varepsilon_{\mathrm{r}}}$ *to the discrete curl–curl source problem* (2.11) *and it satisfies the bound*

$$\|\boldsymbol{u}^h\|_{\boldsymbol{V}} + \|p_h\|_Q \leq C \|\boldsymbol{f}\|_{L^2(\Omega)^3}$$

for $C := (C_{\mathrm{dF}}^2 + 1)\varepsilon_\infty$.

Proof. We recall the proof of Theorem 2.1.4 and note that the requirement (2.9) guarantees coercivity of a on $\boldsymbol{V}^h_{\varepsilon_{\mathrm{r}}}$ and that the requirement $\boldsymbol{\nabla} Q_h \subset \boldsymbol{V}^h$ suffices to prove the inf–sup–condition. □

Remark 2.1.9. Note that $\boldsymbol{V}^h_{\varepsilon_{\mathrm{r}}} \not\subseteq \boldsymbol{V}_{\varepsilon_{\mathrm{r}}}$, thus the required inequality cannot be derived from (2.9). It will be formulated as an assumption in Assumption 2.1.13 and later be proved in Lemma 2.1.23.

In analogy to Theorem 2.1.5 we have the following consequence.

Theorem 2.1.10. *The mapping* $\boldsymbol{T}^h : L^2(\Omega)^3 \to \boldsymbol{V}^h_{\varepsilon_\mathrm{r}} \subset \boldsymbol{V}^h \subset H(\mathrm{curl},\Omega)$, $\boldsymbol{f} \mapsto \boldsymbol{T}^h\boldsymbol{f} := \boldsymbol{u}^h$ *with* $\boldsymbol{u}^h$ *from Theorem* 2.1.8 *is linear, continuous, and compact.*

Proof. This is a direct consequence of the previous Theorem 2.1.8. The compactness is trivial since $\boldsymbol{V}^h_{\varepsilon_\mathrm{r}}$ is finite dimensional. □

2.1.4 Problems of Maxwell eigenvalue computations

(1) Solutions in general Lipschitz domains can have strong singularities: if Φ is a solution to $\Delta\Phi = 0$ in an L–shaped domain Ω we have $\boldsymbol{\nabla}\Phi \in H^s(\Omega)^3$ for some $s \in (\frac{1}{2}, 1)$. Since $\boldsymbol{\nabla} \times \boldsymbol{\nabla}\Phi = 0$ and $\boldsymbol{\nabla} \cdot \boldsymbol{\nabla}\Phi = 0$, $\boldsymbol{u} = \boldsymbol{\nabla}\Phi$ is an example of a singular solution of a curl–curl equation. In case of discontinuous permittivities, however, one may find examples that $\boldsymbol{u} \in H^s(\Omega)^3$ for any given $s > 0$ [14].

(2) The operator curl has an infinite dimensional kernel, namely the space of all gradients (here $\boldsymbol{\nabla}H^1_0(\Omega)$). The relevant eigenfunctions however lie in the orthogonal component to these gradients. This has been used for the coercivity estimate and for the inf–sup condition in the proof of Theorem 2.1.4.

(3) Finite elements space that do not fit to the curl–div structure will in general produce spurious eigenvalues since the gradient space is not well separated from its orthogonal component [2, Sect. 5].

(4) If one uses H^1–conforming spaces, the method will only compute the projection of the singular solution into $H^1(\Omega)^3$ since the ansatz space is only a proper subspace of the solution space: the method seems to converge, the result however is wrong [12] [26, Lem. 3.5.6] [2, Sect. 5].

2.1.5 Convergence of discrete eigenvalues

With notations from (2.4)–(2.6), the *discrete curl–curl eigenvalue problem* reads

$$\begin{aligned} a(\boldsymbol{u}^h, \boldsymbol{v}^h) + b(\boldsymbol{v}^h, p_h) &= \lambda_h \int_\Omega \varepsilon_\mathrm{r} \boldsymbol{u}^h \cdot \boldsymbol{v}^h \qquad && \text{for all } \boldsymbol{v}^h \in \boldsymbol{V}^h, \\ b(\boldsymbol{u}^h, q_h) &= 0 && \text{for all } q_h \in Q_h. \end{aligned}$$

An abstract framework

With the operator $\boldsymbol{T}^h$ from Section 2.1.3 at hand, the discrete eigenvalue problem can be formulated as $\boldsymbol{T}^h(\lambda_h \boldsymbol{u}^h) = \boldsymbol{u}^h$ or $\boldsymbol{T}^h\boldsymbol{u}^h = 1/\lambda_h\, \boldsymbol{u}^h$ for $\lambda_h \neq 0$. The convergence of the eigenvalues λ_h for h to 0 is connected to the convergence of eigenvalues of $\boldsymbol{T}^h$ towards eigenvalues of $\boldsymbol{T}$. For linear spaces X, Y, $I\!L(X, Y)$ will denote the space of linear mappings $X \to Y$ together with the operator norm.

Theorem 2.1.11. *For the uniform convergence of the spectrum of* $\boldsymbol{T}^h$ *towards the spectrum of* $\boldsymbol{T}$ *it is necessary and sufficient that*

$$\lim_{h\to 0} \|\boldsymbol{T} - \boldsymbol{T}^h\|_{I\!L(L^2(\Omega)^3, L^2(\Omega)^3)} = 0.$$

Proof. [6, p. 1288] □

Theorem 2.1.12. *Assume that* $\|\boldsymbol{T} - \boldsymbol{T}^h\|_{\mathbb{L}(L^2(\Omega)^3, L^2(\Omega)^3)} \leq Ch^t$ *for* $h \leq h_0$ *with some* $h_0, t > 0$. *Let* $\lambda \in \mathbb{C} \setminus \{0\}$ *be an eigenvalue of* $\boldsymbol{T}$ *with multiplicity* $m_j \in \mathbb{N}$ *and eigenspace* $\mathcal{E}(\lambda_j) \subset \boldsymbol{V}_{\varepsilon_r}$. *Then there are exactly* m_j *discrete eigenvalues* $\lambda_{h,j_1} \dots \lambda_{h,j_m}$ *of* $\boldsymbol{T}^h$ *that converge to* λ_j. *If we define the approximate eigenvalue by*

$$\widetilde{\lambda}_{h,j} := \frac{1}{m_j} \sum_{l=1}^{m_j} \lambda_{h,j_l}$$

and the corresponding approximate eigenspace in $\boldsymbol{V}^h_{\varepsilon_r}$ *by*

$$\widetilde{\mathcal{E}}^h(\lambda_{h,j}) := \bigoplus_{l=1}^{m_j} \mathcal{E}^h(\lambda_{h,j_l}),$$

then there exist $h_0 > 0$ *such that for all* $h \in (0, h_0)$

$$|\widetilde{\lambda}_j - \widetilde{\lambda}_{h,j}| \leq Ch^{2t} \quad \text{and} \quad \delta(\mathcal{E}(\lambda_j), \widetilde{\mathcal{E}}^h(\lambda_{h,j})) \leq Ch^t,$$

where δ *measures the distance between linear spaces.*

Proof. See e. g. [3], [6, Thm. 1]. □

Convergence of the discrete curl–curl source problem

Following [6] (or [2, Sect. 13]), we now establish the convergence of solutions of the discrete curl–curl source problem (2.11) towards those of (2.2) under sufficient conditions that are formulated in the following assumption. Here, we slightly changed condition (3) and separated it from the regularity requirement (4) for solutions of Maxwell equations.

For convenience we introduce, for $r, s \geq 0$, the space

$$H^{(r,s)}(\mathrm{curl}, \Omega) := \{\boldsymbol{v} \in H^r(\Omega)^3 \,:\, \boldsymbol{\nabla} \times \boldsymbol{v} \in H^s(\Omega)^3\}$$

with the norm, resp. semi-norm,

$$\begin{aligned} \|\boldsymbol{v}\|_{H^{(r,s)}(\mathrm{curl},\Omega)} &:= \|\boldsymbol{v}\|_{H^r(\Omega)^3} + \|\boldsymbol{\nabla} \times \boldsymbol{v}\|_{H^s(\Omega)^3}, \\ [\![\boldsymbol{v}]\!]_{H^{(r,s)}(\mathrm{curl},\Omega)} &:= [\![\boldsymbol{v}]\!]_{H^r(\Omega)^3} + [\![\boldsymbol{\nabla} \times \boldsymbol{v}]\!]_{H^s(\Omega)^3}. \end{aligned}$$

For $r = s$ we let $H^{(r,r)}(\mathrm{curl}, \Omega) = H^r(\mathrm{curl}, \Omega)$.

Assumption 2.1.13 (Convergence requirements).

(1) *Ellipticity on the discrete kernel*: Assume that there exists a constant $C_{\mathrm{dF}} > 0$ such that

$$\|\boldsymbol{v}^h\|_{L^2(\Omega)^3} \leq C_{\mathrm{dF}} \|\boldsymbol{\nabla} \times \boldsymbol{v}^h\|_{L^2(\Omega)^3} \tag{2.12}$$

holds for all $\boldsymbol{v}^h \in \boldsymbol{V}^h_{\varepsilon_{\mathrm{r}}}$.

(2) *Weak approximability*: For some $s > 0$ holds that for all $\boldsymbol{v}^h \in \boldsymbol{V}^h_{\varepsilon_{\mathrm{r}}}$ there exists $\boldsymbol{v} \in \boldsymbol{V}_{\varepsilon_{\mathrm{r}}}$ such that

$$\|\boldsymbol{v}^h - \boldsymbol{v}\|_{L^2(\Omega)^3} \leq C h^s \|\boldsymbol{\nabla} \times \boldsymbol{v}^h\|_{L^2(\Omega)^3}. \tag{2.13}$$

(3) *Strong approximability*: For some $r, r' > 0$ holds that for all suitably regular $\boldsymbol{v} \in \boldsymbol{V}$, there exists $\boldsymbol{v}^h \in \boldsymbol{V}^h$ such that

$$\|\boldsymbol{v} - \boldsymbol{v}^h\|_{\boldsymbol{V}} \leq C h^r \begin{cases} \|\boldsymbol{v}\|_{H^{(r,r')}(\mathrm{curl},\Omega)} & \text{for } r,\, r' > 0, \\ \|\boldsymbol{v}\|_{H^r(\Omega)^3} & \text{for } r > 1. \end{cases} \tag{2.14}$$

(4) *Regularity*: For the solution $\boldsymbol{u} = \boldsymbol{T}\boldsymbol{f} \in \boldsymbol{V}_{\varepsilon_{\mathrm{r}}}$ of the weak curl–curl problem (2.2) holds one of the a priori bounds

$$\begin{aligned} &\|\boldsymbol{u}\|_{H^{(r,r')}(\mathrm{curl},\Omega)} \leq C\|\boldsymbol{f}\|_{L^2(\Omega)^3} \quad \text{for } r,\, r' > 0 \\ \text{or} \qquad &\|\boldsymbol{u}\|_{H^r(\Omega)^3} \leq C\|\boldsymbol{f}\|_{L^2(\Omega)^3} \quad \text{for } r > 1. \end{aligned}$$

Remark 2.1.14. The interpolation estimate (2.14) can actually be obtained with $\|\boldsymbol{v}\|_{H^r(\Omega)^3} + \|\boldsymbol{\nabla} \times \boldsymbol{v}\|_{L^p(\Omega)}$, for $p > 2$, on the right hand side [6, p. 1286]. For $r > 1$, this last term can be estimated by $\|\boldsymbol{v}\|_{H^r(\Omega)^3}$ using Sobolev embedding results, Section 1.1.4.

The basic error estimate can now be formulated as follows, a result often called Strang lemma in finite element theory [17, Ch. 2.3.2], see also [3].

Lemma 2.1.15. *Using Assumption* 2.1.13. (1) *we have the error bound*

$$\|\boldsymbol{u} - \boldsymbol{u}^h\|_{\boldsymbol{V}} \leq C\Big(\inf_{\boldsymbol{v}^h \in \boldsymbol{V}^h} \|\boldsymbol{u} - \boldsymbol{v}^h\|_{\boldsymbol{V}} + \sup_{\boldsymbol{w}^h \in \boldsymbol{V}^h_{\varepsilon_{\mathrm{r}}}} \inf_{\boldsymbol{w} \in \boldsymbol{V}_{\varepsilon_{\mathrm{r}}}} \frac{|b(p, \boldsymbol{w}^h - \boldsymbol{w})|}{\|\boldsymbol{\nabla} \times \boldsymbol{w}^h\|_{L^2(\Omega)^3}} \Big)$$

between the solutions of the continuous and discrete curl–curl source problem, $\boldsymbol{u} = \boldsymbol{T}\boldsymbol{f} \in \boldsymbol{V}_{\varepsilon_{\mathrm{r}}}$ *and* $\boldsymbol{u}^h = \boldsymbol{T}^h\boldsymbol{f} \in \boldsymbol{V}^h_{\varepsilon_{\mathrm{r}}}$ *(for* $\boldsymbol{f} \in L^2(\Omega)^3$*), respectively. The constant* C *can be chosen as* $(C_{\mathrm{dF}} + 2)(1 + \sqrt{\varepsilon_\infty})$.

Proof. Let $[\boldsymbol{u}, p] \in \boldsymbol{V}_{\varepsilon_\mathrm{r}} \times Q$ and $[\boldsymbol{u}^h, p_h] \in \boldsymbol{V}^h_{\varepsilon_\mathrm{r}} \times Q_h$ solve (2.2) and (2.11), respectively. We start to bound $\|\boldsymbol{v}^h - \boldsymbol{u}^h\|_{\boldsymbol{V}}$ for arbitrary $\boldsymbol{v}^h \in \boldsymbol{V}^h_{\varepsilon_\mathrm{r}}$ and get

$$\begin{aligned}
\|\boldsymbol{\nabla} \times (\boldsymbol{v}^h - \boldsymbol{u}^h)\|^2_{L^2(\Omega)^3} &= \int_\Omega \boldsymbol{\nabla} \times (\boldsymbol{v}^h - \boldsymbol{u}^h) \cdot \boldsymbol{\nabla} \times (\boldsymbol{v}^h - \boldsymbol{u}^h) \\
&= \int_\Omega \boldsymbol{\nabla} \times \big(\boldsymbol{v}^h - \boldsymbol{u} + \boldsymbol{u} - \boldsymbol{u}^h\big) \cdot \boldsymbol{\nabla} \times (\boldsymbol{v}^h - \boldsymbol{u}^h) \\
&\leq \|\boldsymbol{\nabla} \times (\boldsymbol{v}^h - \boldsymbol{u})\|_{L^2(\Omega)^3} \|\boldsymbol{\nabla} \times (\boldsymbol{v}^h - \boldsymbol{u}^h)\|_{L^2(\Omega)^3} + \big|b(p - p_h, \boldsymbol{v}^h - \boldsymbol{u}^h)\big|,
\end{aligned}$$

hence with $b(p - p_h, \boldsymbol{v}^h - \boldsymbol{u}^h) = b(p, \boldsymbol{v}^h - \boldsymbol{u}^h - \boldsymbol{w})$ for arbitrary $\boldsymbol{w} \in \boldsymbol{V}_{\varepsilon_\mathrm{r}}$

$$\begin{aligned}
\big|b(p - p_h, \boldsymbol{v}^h - \boldsymbol{u}^h)\big| &\leq \inf_{\boldsymbol{w} \in \boldsymbol{V}_{\varepsilon_\mathrm{r}}} \big|b(p, \boldsymbol{v}^h - \boldsymbol{u}^h - \boldsymbol{w})\big| \\
&\leq \sup_{\boldsymbol{w}^h \in \boldsymbol{V}^h_{\varepsilon_\mathrm{r}}} \inf_{\boldsymbol{w} \in \boldsymbol{V}_{\varepsilon_\mathrm{r}}} \frac{|b(p, \boldsymbol{w}^h - \boldsymbol{w})|}{\|\boldsymbol{\nabla} \times \boldsymbol{w}^h\|_{L^2(\Omega)^3}} \|\boldsymbol{\nabla} \times (\boldsymbol{v}^h - \boldsymbol{u}^h)\|_{L^2(\Omega)^3}.
\end{aligned}$$

This gives

$$\|\boldsymbol{\nabla} \times (\boldsymbol{v}^h - \boldsymbol{u}^h)\|_{L^2(\Omega)^3} \leq \|\boldsymbol{\nabla} \times (\boldsymbol{v}^h - \boldsymbol{u})\|_{L^2(\Omega)^3} + \sup_{\boldsymbol{w}^h \in \boldsymbol{V}^h_{\varepsilon_\mathrm{r}}} \inf_{\boldsymbol{w} \in \boldsymbol{V}_{\varepsilon_\mathrm{r}}} \frac{|b(p, \boldsymbol{w}^h - \boldsymbol{w})|}{\|\boldsymbol{\nabla} \times \boldsymbol{w}^h\|_{L^2(\Omega)^3}}.$$

The assertion with $\inf_{\boldsymbol{v}^h \in \boldsymbol{V}^h_{\varepsilon_\mathrm{r}}}$ follows from

$$\begin{aligned}
\|\boldsymbol{u} - \boldsymbol{u}^h\|_{\boldsymbol{V}} &\leq \|\boldsymbol{u} - \boldsymbol{v}^h\|_{\boldsymbol{V}} + \|\boldsymbol{v}^h - \boldsymbol{u}^h\|_{\boldsymbol{V}} \\
&\leq \|\boldsymbol{u} - \boldsymbol{v}^h\|_{\boldsymbol{V}} + (C_\mathrm{dF} + 1)\|\boldsymbol{\nabla} \times (\boldsymbol{v}^h - \boldsymbol{u}^h)\|_{L^2(\Omega)^3} \\
&\leq (C_\mathrm{dF} + 2)\|\boldsymbol{u} - \boldsymbol{v}^h\|_{\boldsymbol{V}} + (C_\mathrm{dF} + 1) \sup_{\boldsymbol{w}^h \in \boldsymbol{V}^h_{\varepsilon_\mathrm{r}}} \inf_{\boldsymbol{w} \in \boldsymbol{V}_{\varepsilon_\mathrm{r}}} \frac{|b(p, \boldsymbol{w}^h - \boldsymbol{w})|}{\|\boldsymbol{\nabla} \times \boldsymbol{w}^h\|_{L^2(\Omega)^3}}.
\end{aligned}$$

Now let $\boldsymbol{v}^h \in \boldsymbol{V}^h$ and define $\boldsymbol{z_h} = \boldsymbol{\nabla}\phi_h$ by $\int_\Omega \varepsilon_r \boldsymbol{\nabla}\phi_h \cdot \boldsymbol{\nabla} q_h = \int_\Omega \varepsilon_r (\boldsymbol{u} - \boldsymbol{v}^h) \cdot \boldsymbol{\nabla} q_h$ for all $q_h \in Q_h$. $\boldsymbol{z}^h$ uniquely exists with $\|\boldsymbol{z}^h\|_{L^2(\Omega)^3} \leq \sqrt{\varepsilon_\infty}\|\boldsymbol{u} - \boldsymbol{v}^h\|_{L^2(\Omega)^3}$. But then $\boldsymbol{v}^h + \boldsymbol{z}^h \in \boldsymbol{V}^h_{\varepsilon_\mathrm{r}}$ and

$$\|\boldsymbol{u} - (\boldsymbol{v}^h + \boldsymbol{z}^h)\|_{\boldsymbol{V}} \leq \|\boldsymbol{u} - \boldsymbol{v}^h\|_{\boldsymbol{V}} + \|\boldsymbol{z}^h\|_{L^2(\Omega)^3} \leq (1 + \sqrt{\varepsilon_\infty})\|\boldsymbol{u} - \boldsymbol{v}^h\|_{\boldsymbol{V}}.$$

This shows the assertion with $\inf_{\boldsymbol{v}^h \in \boldsymbol{V}^h}$. □

Now we can prove an error estimation under the condition that $\boldsymbol{u}$ is sufficiently regular as stated in Assumptions 2.1.13.(4) (cf. [6]).

Theorem 2.1.16. *Under Assumptions* 2.1.13 *we have* $\boldsymbol{T}^h \to \boldsymbol{T}$ *for* $h \to 0$ *in* $\mathbb{L}(L^2(\Omega)^3, L^2(\Omega)^3)$*, and more precisely, with* $t := \min\{r, s\}$*,*

$$\|\boldsymbol{T}\boldsymbol{f} - \boldsymbol{T}^h\boldsymbol{f}\|_{\boldsymbol{V}} \leq Ch^t \|\boldsymbol{f}\|_{L^2(\Omega)^3}.$$

Thus the assertions of Theorem 2.1.12 *hold true and the convergence of the eigenvalues and eigenspaces can be deduced accordingly.*

Proof. We proceed with the result from Lemma 2.1.15 in order to establish an estimate for $\|\boldsymbol{u}-\boldsymbol{u}^h\|_{\boldsymbol{V}}$ in terms of $\|\boldsymbol{f}\|_{L^2(\Omega)^3}$.

Given $\boldsymbol{w}^h$, we see from Assumption 2.1.13.(2) that we can find $\boldsymbol{w} \in \boldsymbol{V}_{\varepsilon_\mathrm{r}}$ such that

$$\frac{|b(p,\boldsymbol{w}^h-\boldsymbol{w})|}{\|\boldsymbol{\nabla}\times\boldsymbol{w}^h\|_{L^2(\Omega)^3}} \le \varepsilon_\infty \frac{\|\boldsymbol{w}^h-\boldsymbol{w}\|_{L^2(\Omega)^3}}{\|\boldsymbol{\nabla}\times\boldsymbol{w}^h\|_{L^2(\Omega)^3}} \|p\|_Q \le Ch^s \|\boldsymbol{f}\|_{L^2(\Omega)^3}$$

for some $s>0$. Thanks to Assumption 2.1.13.(3-4) we can choose $\boldsymbol{v}^h$ so that

$$\|\boldsymbol{u}-\boldsymbol{v}^h\|_{\boldsymbol{V}} \le Ch^r \|\boldsymbol{f}\|_{L^2(\Omega)^3}, \tag{2.15}$$

where one of the cases $r\in(0,1]$ or $r>1$ is used. This proves

$$\|\boldsymbol{u}-\boldsymbol{u}^h\|_{\boldsymbol{V}} \le Ch^{\min\{r,s\}} \|\boldsymbol{f}\|_{L^2(\Omega)^3}. \qquad \square$$

Verification of Assumptions 2.1.13

We start with a modification of the Helmholtz decomposition Theorem 1.2.3 for nonconstant ε_r and a discrete version of it.

Theorem 2.1.17. *Let $\Omega\subset\mathbb{R}^3$ and ε_r as in Assumption 2.1.1. For each $\boldsymbol{v}\in\boldsymbol{V}$, there exists $\boldsymbol{z}\in\boldsymbol{V}_{\varepsilon_\mathrm{r}}$ and $q\in H_0^1(\Omega)$ such that*

$$\boldsymbol{v} = \boldsymbol{z} + \boldsymbol{\nabla} q.$$

This splitting is orthogonal with respect to the ε_r-weighted $L^2(\Omega)^3$ and the $H(\mathrm{curl},\Omega)$ inner product. The mappings $\boldsymbol{v}\mapsto\boldsymbol{z}$ and $\boldsymbol{v}\mapsto\boldsymbol{\nabla}q$ are continuous, that is, it holds

$$\|\boldsymbol{z}\|_{\boldsymbol{V}} + \|\boldsymbol{\nabla}q\|_{L^2(\Omega)^3} \le \|\boldsymbol{v}\|_{\boldsymbol{V}}.$$

Proof. See Theorem 1.2.3 or [26, Lem. 4.5]. $\square$

Corollary 2.1.18. *Let $\Omega\subset\mathbb{R}^3$ and ε_r as in Assumption 2.1.1. For each $\boldsymbol{v}\in\boldsymbol{V}$, there exists a unique $\boldsymbol{w}\in\boldsymbol{V}_{\varepsilon_\mathrm{r}}$ such that*

$$\boldsymbol{\nabla}\times\boldsymbol{w} = \boldsymbol{\nabla}\times\boldsymbol{v} \quad \text{in } \Omega.$$

Moreover, it holds $\boldsymbol{w}\in H^s(\Omega)^3$ for some $s>0$ with the bound

$$\|\boldsymbol{w}\|_{H^s(\Omega)^3} \le C\|\boldsymbol{v}\|_{\boldsymbol{V}}$$

for some constant $C>0$. If ε_r is uniformly Lipschitz-continuous, then $s>1/2$. If, in addition to that, Ω is convex, then we can take $s=1$. The mapping $\boldsymbol{v}\mapsto\boldsymbol{w}:=H_{\varepsilon_\mathrm{r}}\boldsymbol{v}$ is also called Hodge mapping [19, Ch. 4.2].

Proof. We apply Theorem 2.1.17 to $\boldsymbol{v} \in \boldsymbol{V}$ and define $\boldsymbol{w} := \boldsymbol{z} \in \boldsymbol{V}_{\varepsilon_\mathrm{r}}$. The first assertion then follows immediately. The second assertion then is verified using Theorem 2.1.2. □

Theorem 2.1.19. *Let $\Omega \subset \mathbb{R}^3$ and ε_r as in Assumption* 2.1.1. *Let $\boldsymbol{V}^h$ and Q_h as in Section* 2.1.3 *with $\boldsymbol{\nabla} Q_h \subset \boldsymbol{V}^h$. Then, for each $\boldsymbol{v}^h \in \boldsymbol{V}^h$, there exists $\boldsymbol{z}^h \in \boldsymbol{V}^h_{\varepsilon_\mathrm{r}}$ and $q_h \in Q_h$ such that*

$$\boldsymbol{v}^h = \boldsymbol{z}^h + \boldsymbol{\nabla} q_h.$$

This splitting is orthogonal with respect to the ε_r-weighted $L^2(\Omega)^3$ and the $H(\mathrm{curl}, \Omega)$ inner product. The mappings $\boldsymbol{v}^h \mapsto \boldsymbol{z}^h$ and $\boldsymbol{v}^h \mapsto \boldsymbol{\nabla} q_h$ are continuous, that is, it holds

$$\|\boldsymbol{z}^h\|_{H(\mathrm{curl},\Omega)} + \|\boldsymbol{\nabla} q_h\|_{L^2(\Omega)^3} \leq \|\boldsymbol{v}^h\|_{H(\mathrm{curl},\Omega)}.$$

Proof. See Theorem 1.2.3 for the proof or [26, Lem. 4.5]. □

To proceed, we first need some more specific assumptions on the discrete spaces formulated below. It is assumed that our finite element space $\boldsymbol{V}^h$ is constructed on a collection of elements $\mathcal{T}$ of tetrahedra or hexahedra denoted by T with the usual requirements [8, Ch. 3], [17, Ch. 1.2]. In our case we can require $\overline{\Omega} = \cup_{T\in\mathcal{T}} T$. For $T \in \mathcal{T}$ we let $h_T := \mathrm{diam}(T)$ be the diameter of an element T and ω_T be the local domain composed of T and all its neighbouring elements, $\omega_T := \cup_{T'\in\mathcal{T}\,:\,T'\cap T\neq\emptyset}\{T'\}$. Note that $h = \max_{T\in\mathcal{T}} h_T$. It is assumed that the mesh is quasi-uniform, meaning that $h_T/h_{T'} \leq C$ for all $T' \in \omega_T$ and all $T \in \mathcal{T}$ with a universal constant $C > 0$.

Assumption 2.1.20. Assume that for $\boldsymbol{V}^h$ there exists a linear projection $\boldsymbol{\Pi}^h : \boldsymbol{V} \cap H^{s_0}(\Omega)^3 \to \boldsymbol{V}^h$, for some $s_0 \in (0, 1]$, such that

(1) $\boldsymbol{\Pi}^h \boldsymbol{v}^h = \boldsymbol{v}^h$ for all $\boldsymbol{v}^h \in \boldsymbol{V}^h$,

(2) $\boldsymbol{\nabla} \times \boldsymbol{v} = \boldsymbol{0}$ implies $\boldsymbol{\Pi}^h \boldsymbol{v} \in \boldsymbol{\nabla} Q_h$ for all $\boldsymbol{v} \in \boldsymbol{V}$,

(3) For all sufficiently regular $\boldsymbol{v}$ holds

$$\|\boldsymbol{v} - \boldsymbol{\Pi}^h \boldsymbol{v}\|_{L^2(T)^3} \leq C h_T^r \begin{cases} [\![\boldsymbol{v}]\!]_{H^{(r,r')}(\mathrm{curl},\omega_T)} & \text{for } r \in [s_0, 1],\ r' > 0, \\ [\![\boldsymbol{v}]\!]_{H^r(\omega_T)^3} & \text{for } r > 1, \end{cases}$$

$$\|\boldsymbol{\nabla} \times (\boldsymbol{v} - \boldsymbol{\Pi}^h \boldsymbol{v})\|_{L^2(T)^3} \leq C h_T^r [\![\boldsymbol{\nabla} \times \boldsymbol{v}]\!]_{H^r(\omega_T)^3} \quad \text{for } r \geq s_0$$

(cf. Section 1.2.2). Moreover, if $\boldsymbol{\nabla} \times \boldsymbol{v}$ is piecewise polynomial on $\mathcal{T}$, then

$$\|\boldsymbol{v} - \boldsymbol{\Pi}^h \boldsymbol{v}\|_{L^2(T)^3} \leq C\big(h_T^s [\![\boldsymbol{v}]\!]_{H^s(\omega_T)^3} + h_T \|\boldsymbol{\nabla} \times \boldsymbol{v}\|_{L^2(\omega_T)^3}\big) \tag{2.16}$$

for some $s \in [s_0, 1]$.

Lemma 2.1.21 (Strong approximability). *Let $\boldsymbol{V}^h$ satisfy Assumption* 2.1.20. *Then the strong approximability* 2.1.13. (3) *is valid for $r \geq s_0$.*

Proof. Use Assumption 2.1.20.(3) and sum its square up over $T \in \mathcal{T}$. □

Lemma 2.1.22 (Weak approximability). *Let $\boldsymbol{V}^h$ satisfy Assumption* 2.1.20. *Then the weak approximability* 2.1.13. (2) *is valid for $s \geq s_0$.*

Proof. (Cf. [19, Lem. 4.5]) Let $\boldsymbol{v}^h \in \boldsymbol{V}^h_{\varepsilon_\mathrm{r}}$ be given. Define $\boldsymbol{v} \in \boldsymbol{V}_{\varepsilon_\mathrm{r}}$ by $\boldsymbol{v} = H_{\varepsilon_\mathrm{r}} \boldsymbol{v}^h \in H^s(\Omega)^3$ as in Corollary 2.1.18 for some $s \geq s_0$. By Assumption 2.1.20.(1) we have $\boldsymbol{v}^h - \boldsymbol{\Pi}^h \boldsymbol{v} = \boldsymbol{\Pi}^h(\boldsymbol{v}^h - \boldsymbol{v})$ and by definition $\boldsymbol{\nabla} \times (\boldsymbol{v}^h - \boldsymbol{v}) = \boldsymbol{0}$ which implies that $\boldsymbol{v}^h - \boldsymbol{\Pi}^h \boldsymbol{v} = \boldsymbol{\nabla} q_h$ for some $q_h \in Q_h$ by Assumption 2.1.20.(2). Thus we can derive the bound (note $Q_h \subset Q$)

$$\begin{aligned}
\|\sqrt{\varepsilon_\mathrm{r}}(\boldsymbol{v}^h - \boldsymbol{v})\|^2_{L^2(\Omega)^3} &= \int_\Omega \varepsilon_\mathrm{r}(\boldsymbol{v}^h - \boldsymbol{v}) \cdot (\boldsymbol{v}^h - \boldsymbol{\Pi}^h \boldsymbol{v} + \boldsymbol{\Pi}^h \boldsymbol{v} - \boldsymbol{v}) \\
&= \int_\Omega \varepsilon_\mathrm{r}(\boldsymbol{v}^h - \boldsymbol{v}) \cdot (\boldsymbol{\Pi}^h \boldsymbol{v} - \boldsymbol{v}) \\
&\leq \sqrt{\varepsilon_\infty}\, \|\sqrt{\varepsilon_\mathrm{r}}(\boldsymbol{v}^h - \boldsymbol{v})\|_{L^2(\Omega)^3} \|\boldsymbol{\Pi}^h \boldsymbol{v} - \boldsymbol{v}\|_{L^2(\Omega)^3}
\end{aligned}$$

which gives

$$\|\boldsymbol{v}^h - \boldsymbol{v}\|_{L^2(\Omega)^3} \leq \|\sqrt{\varepsilon_\mathrm{r}}(\boldsymbol{v}^h - \boldsymbol{v})\|^2_{L^2(\Omega)^3} \leq \sqrt{\varepsilon_\infty}\, \|\boldsymbol{\Pi}^h \boldsymbol{v} - \boldsymbol{v}\|_{L^2(\Omega)^3}.$$

Now observe that $\boldsymbol{\nabla} \times \boldsymbol{v} = \boldsymbol{\nabla} \times \boldsymbol{v}^h$ is piecewise polynomial so that for some $s \geq s_0$

$$\|\boldsymbol{v}^h - \boldsymbol{v}\|_{L^2(\Omega)^3} \leq Ch^s \big([\![\boldsymbol{v}]\!]_{H^s(\Omega)^3} + \|\boldsymbol{\nabla} \times \boldsymbol{v}\|_{L^2(\Omega)^3} \big) \leq Ch^s \|\boldsymbol{\nabla} \times \boldsymbol{v}^h\|_{L^2(\Omega)^3},$$

where we have used Assumption 2.1.20.(3) ((2.16) squared and summed up over $T \in \mathcal{T}$) and the bound $[\![\boldsymbol{v}]\!]_{H^s(\Omega)^3} \leq C \|\boldsymbol{\nabla} \times \boldsymbol{v}\|_{L^2(\Omega)^3}$ resulting from Theorem 2.1.2 and Theorem 2.1.3. This gives the stated result. □

Lemma 2.1.23 (Ellipticity on the discrete kernel). *Let $\boldsymbol{V}^h$ satisfy Assumption* 2.1.20. *Then the ellipticity on the discrete kernel* 2.1.13. (1) *is valid.*

Proof. (Cf. [19, Lem. 4.7]) Let $\boldsymbol{v}^h \in \boldsymbol{V}^h_{\varepsilon_\mathrm{r}}$. According to Theorem 2.1.17 and Theorem 2.1.19 there exists $\boldsymbol{z} \in \boldsymbol{V}_1$, $q \in Q$ and $\boldsymbol{z}^h \in \boldsymbol{V}^h_1$ (that is, with permittivity 1!), $q_h \in Q_h$ such that $\boldsymbol{v}^h = \boldsymbol{z} + \boldsymbol{\nabla} q$ and $\boldsymbol{v}^h = \boldsymbol{z}^h + \boldsymbol{\nabla} q_h$. With this we get the estimate

$$\begin{aligned}
\|\sqrt{\varepsilon_\mathrm{r}} \boldsymbol{v}^h\|^2_{L^2(\Omega)^3} &= \int_\Omega \varepsilon_\mathrm{r} \boldsymbol{v}^h \cdot \boldsymbol{v}^h = \int_\Omega \varepsilon_\mathrm{r} \boldsymbol{v}^h \cdot \boldsymbol{z}^h \\
&\leq \sqrt{\varepsilon_\infty}\, \|\sqrt{\varepsilon_\mathrm{r}} \boldsymbol{v}^h\|_{L^2(\Omega)^3} \big(\|\boldsymbol{z}\|_{L^2(\Omega)^3} + \|\boldsymbol{z} - \boldsymbol{z}^h\|_{L^2(\Omega)^3} \big).
\end{aligned}$$

The estimate $\|\boldsymbol{z}\|_{L^2(\Omega)^3} \leq C_\mathrm{F} \|\boldsymbol{\nabla} \times \boldsymbol{z}\|_{L^2(\Omega)^3}$ follows from Theorem 2.1.3. Observe that $\boldsymbol{\nabla} \times \boldsymbol{z} = \boldsymbol{\nabla} \times \boldsymbol{z}^h = \boldsymbol{\nabla} \times \boldsymbol{v}^h$ by construction, so that actually it holds that $\boldsymbol{z} = H_{\varepsilon_\mathrm{r}} \boldsymbol{z}^h$. From the proof of the weak approximability, Lemma 2.1.22, we thus get $\|\boldsymbol{z} - \boldsymbol{z}^h\|_{L^2(\Omega)^3} \leq Ch^s \|\boldsymbol{\nabla} \times \boldsymbol{z}^h\|_{L^2(\Omega)^3}$ for some $s > 0$. By insertion of these equalities and inequalities we end up with the stated result. □

Theorem 2.1.24 (Regularity of the electric field). *Let $\boldsymbol{f} \in L^2(\Omega)^3$. Then for the solution $\boldsymbol{E} = \boldsymbol{T}\boldsymbol{f} \in \boldsymbol{V}_{\varepsilon_\mathrm{r}}$ of the weak curl–curl problem* (2.2) *holds the priori bound*

$$\|\boldsymbol{E}\|_{H^{(r',r'')}(\mathrm{curl},\Omega)} \leq C\|\boldsymbol{f}\|_{L^2(\Omega)^3} \quad \text{for some } r' > 0,\ r'' > 1/2.$$

Proof. (Cf. [26, Lem. 7.7]) We first note that the estimate for $\|\boldsymbol{E}\|_{H^{r'}(\Omega)^3}$, for some $r' > 0$, is a consequence of Theorem 2.1.2. Thus it remains to prove a corresponding estimate for $\boldsymbol{w} := \boldsymbol{\nabla} \times \boldsymbol{E}$. For arbitrary $\boldsymbol{f}$, the solution $\boldsymbol{E}$ of (2.2) satisfies $\boldsymbol{\nabla} \times \boldsymbol{w} = \boldsymbol{\nabla} \times \boldsymbol{\nabla} \times \boldsymbol{E} = \varepsilon_\mathrm{r}(\boldsymbol{f} - \boldsymbol{\nabla} p)$ and this right hand side is in $L^2(\Omega)^3$ by assumption and Theorem 2.1.4. Hence $\boldsymbol{w} \in H(\mathrm{curl}, \Omega)$ and furthermore $\boldsymbol{\nabla} \cdot \boldsymbol{w} = 0$. Therefore, the trace $\boldsymbol{n} \cdot \boldsymbol{w}$ is well-defined in $H^{-1/2}(\partial\Omega)$ (Section 1.2.4). We claim $\boldsymbol{n} \cdot \boldsymbol{w} = 0$. This would prove $\boldsymbol{w} \in X_\mathrm{T}$ and by Theorem 1.2.1 that $\boldsymbol{w} \in H^{r''}(\Omega)^3$ for some $r'' > 1/2$ (note that ε_r does not appear in this argument).

Fix $\boldsymbol{x}_0$ so that Ω is smooth near $\boldsymbol{x}_0$. We may represent $\boldsymbol{E}$ as $\boldsymbol{E} = \alpha\boldsymbol{n} + \beta\boldsymbol{t}$, where $\boldsymbol{n}, \boldsymbol{t}$ are extended (into Ω) normal and tangential vector fields with respect to $\partial\Omega$ and α, β some scalar coefficient functions. $\boldsymbol{n}$ is assumed to be a gradient field, i. e., $\boldsymbol{n} \sim \boldsymbol{\nabla}\,\mathrm{dist}(\,.\,, \partial\Omega)$. Due to the boundary condition $\boldsymbol{n} \times \boldsymbol{E} = \boldsymbol{0}$ we have $\beta(\boldsymbol{y}) = 0$ for all $\boldsymbol{y} \in \partial\Omega$. For $\boldsymbol{w}$ we then obtain

$$\begin{aligned}\boldsymbol{n}(\boldsymbol{x}_0) \cdot \boldsymbol{w}(\boldsymbol{x}_0) &= \boldsymbol{n}(\boldsymbol{x}_0) \cdot \Big(\alpha(\boldsymbol{x}_0)\boldsymbol{\nabla} \times \boldsymbol{n}(\boldsymbol{x}_0) + \beta(\boldsymbol{x}_0)\boldsymbol{\nabla} \times \boldsymbol{t}(\boldsymbol{x}_0) \\ &\qquad + \boldsymbol{\nabla}\alpha(\boldsymbol{x}_0) \times \boldsymbol{n}(\boldsymbol{x}_0) + \boldsymbol{\nabla}\beta(\boldsymbol{x}_0) \times \boldsymbol{t}(\boldsymbol{x}_0)\Big) \\ &= \boldsymbol{\nabla}\alpha(\boldsymbol{x}_0) \cdot (\boldsymbol{n}(\boldsymbol{x}_0) \times \boldsymbol{n}(\boldsymbol{x}_0)) + \boldsymbol{t}(\boldsymbol{x}_0) \cdot (\boldsymbol{n}(\boldsymbol{x}_0) \times \boldsymbol{\nabla}\beta(\boldsymbol{x}_0)) = 0.\end{aligned}$$

The last term vanishes since $\boldsymbol{\nabla}\beta(\boldsymbol{x}_0)$ is normal. □

Theorem 2.1.25 (Regularity for time-harmonic fields). *Let $\boldsymbol{E} \in X_\mathrm{N}(\Omega; \varepsilon_\mathrm{r})$ and $\boldsymbol{H} \in X_\mathrm{T}(\Omega; 1)$ be solutions of the time-harmonic Maxwell equations* (1.12)–(1.15). *Then $\boldsymbol{E} \in H^{(r',r'')}(\mathrm{curl}, \Omega)$ with $r' > 0$, $r'' > 1/2$ and $\boldsymbol{H} \in H^{s'}(\Omega)^3$ with $s' > 1/2$, $\boldsymbol{\nabla} \times \boldsymbol{H} \in H^{s''}(K)^3$ with $s'' > 0$ for all $K \subset \Omega$ where ε_r is constant.*

Proof. $\boldsymbol{E}$ is treated as in Theorem 2.1.24. For $\boldsymbol{H}$ we proceed as in the proof of Theorem 2.1.24. Since $\boldsymbol{H} \in X_\mathrm{T}(\Omega; 1)$, we can apply Theorem 1.2.1 to get $\boldsymbol{H} \in H^{s'}(\Omega)^3$ for some $s' > 1/2$. Now define $\boldsymbol{w} := 1/\varepsilon_\mathrm{r}\, \boldsymbol{\nabla} \times \boldsymbol{H}$. Clearly, $\boldsymbol{\nabla} \times \boldsymbol{w} \in L^2(\Omega)^3$, $\boldsymbol{\nabla} \cdot (\varepsilon_\mathrm{r}\boldsymbol{w}) = 0$ in Ω, and $\boldsymbol{n} \times \boldsymbol{w} = \boldsymbol{0}$ on $\partial\Omega$ from (1.12). Hence $\boldsymbol{w} \in H^{s''}(\Omega)^3$ for some $s'' > 0$. This implies $\boldsymbol{\nabla} \times \boldsymbol{H} \in H^{s''}(K)^3$ for all subsets K of Ω where ε_r is constant. □

Remark 2.1.26.

(1) The assertion of the previous theorem applies to the nontrivial eigenfunctions of the eigenvalue problem, or to the solutions to the time-harmonic source problem with a suitable current $\boldsymbol{J}$.

(2) The exponent r' in Theorem 2.1.24 can be arbitrarily small, depending on $\partial\Omega$ and the jump discontinuity of ε_r [14]. If ε_r is Lipschitz-continuous (which

includes the case when ε_r is constant), then $r' > 1/2$ and if moreover Ω is convex, then $r' = 1$, as already denoted in Theorem 2.1.2. If ε_r is piecewise constant on two connected subdomains, then the electric field is piecewise in $(H^{r'})^3$ for $r' \geq 1/4$ and, if Ω is convex, for $r' \geq 1/2$ [14, Sect. 7a]. This holds especially in our applications for photonic crystals, Section 2.2.

The Nédélec edge elements

We now present a family of finite element methods that fulfills the requirements. Take $k \in \mathbb{N}$ and let $\mathcal{P}_k$ be the space of polynomials up to degree k, $\mathcal{P}'_k$ those of homogeneous degree k (i. e. $\mathcal{P}_k = \cup_{l=0}^{k} \mathcal{P}'_l$) and $\mathcal{P}_k^3$ the vector fields with components in $\mathcal{P}_k$. Now one defines

$$\widehat{\boldsymbol{V}}_k := \mathcal{P}_{k-1}^3 \oplus \{\boldsymbol{v} \in (\mathcal{P}'_k)^3 \,:\, \boldsymbol{x} \cdot \boldsymbol{v}(\boldsymbol{x}) = 0 \text{ for all } \boldsymbol{x} \in \mathbb{R}^3\}.$$

This polynomial space satisfies

$$\mathcal{P}_k^3 = \widehat{\boldsymbol{V}}_k \oplus \boldsymbol{\nabla}(\mathcal{P}'_{k+1})^3$$

and for $\boldsymbol{v} \in \widehat{\boldsymbol{V}}_k$ with $\boldsymbol{\nabla} \times \boldsymbol{v} = \boldsymbol{0}$ one gets $\boldsymbol{v} = \boldsymbol{\nabla} q$ for some $q \in \mathcal{P}_{k+1}$.

We let Σ_3 be the standard simplex in $\mathbb{R}^3$ and we consider R_k to be the finite element space on Σ^3. Let $\mathcal{T}$ be the decomposition of Ω into tetrahedra and define for $T \in \mathcal{T}$ a affine linear bijective mapping $\boldsymbol{F}_T : \Sigma_3 \to T$ with $\det(F_T) > 0$. The local finite element space $\boldsymbol{V}_T^h$ on T is then defined by

$$\boldsymbol{V}_T^h := \{\boldsymbol{v} = (D\boldsymbol{F}_T^{\dagger})^{-1} \widehat{\boldsymbol{v}} \circ \boldsymbol{F}_T^{-1} \,:\, \widehat{\boldsymbol{v}} \in \widehat{\boldsymbol{V}}_k\}.$$

A consequence of this definition is that $\boldsymbol{\nabla} \times \boldsymbol{v} = \boldsymbol{0}$ on T is equivalent to $\widehat{\nabla} \times \widehat{\boldsymbol{v}} = \boldsymbol{0}$ on Σ_3. Our global finite element space is now given as

$$\boldsymbol{V}^h := \{\boldsymbol{v} \in H(\mathrm{curl}, \Omega) \,:\, \boldsymbol{v}\big|_T \in \boldsymbol{V}_T^h\}.$$

This will give $\boldsymbol{V}^h \subset H(\mathrm{curl}, \Omega)$ and that the boundary condition $\boldsymbol{n} \times \boldsymbol{v}^h = \boldsymbol{0}$ can be fulfilled. A more detailed description can be found in [26, Ch. 5.5]. The construction of corresponding elements on quadrilaterals is given in [26, Ch. 6.3]. The lowest order method is also described and used in Chapter 2.2.3.

There is a second family of curl-conforming elements on tetrahedra where the local space is $\mathcal{P}_k^3$ [26, Ch. 8.2]. Although they have more degrees of freedom, they do not improve the convergence order in the curl-norm for a given degree. However, they show the improved L^2-convergence which the first family does not provide.

Theorem 2.1.27 (Strong approximation of Nédélec elements 1). *There exists an interpolation operator $\boldsymbol{\Pi}^h : H^{s_0}(\Omega)^3 \to \boldsymbol{V}^h$ that satisfies the conditions of Assumption* 2.1.20 *for $s_0 > 1/2$.*

Proof. It is shown in [26, Thm. 5.41] that for $r = 1/2 + \delta$, $\delta > 0$, one gets

$$\begin{aligned}\|\boldsymbol{v} - \boldsymbol{\Pi}^h \boldsymbol{v}\|_{H(\mathrm{curl},T)} &\leq C h_T^{1/2} \big(h_T^{\delta} \|\boldsymbol{v}\|_{H^{1/2+\delta}(\omega_T)} + h_T^{1/2+\delta} \|\boldsymbol{\nabla} \times \boldsymbol{v}\|_{H^{\delta}(\omega_T)} \big) \\ &\leq C h_T^{r} \big(\|\boldsymbol{v}\|_{H^{r}(\omega_T)} + h_T^{1/2} \|\boldsymbol{\nabla} \times \boldsymbol{v}\|_{H^{r-1/2}(\omega_T)} \big).\end{aligned}$$

Finally this yields for $r > 1/2$

$$\|\boldsymbol{v} - \boldsymbol{\Pi}^h \boldsymbol{v}\|_{\boldsymbol{V}} \leq C h_T^{r} \|\boldsymbol{v}\|_{H^{(r,r-1/2)}(\mathrm{curl},\Omega)}.$$

The remaining properties follow from [26, Ch. 5.5]. □

Theorem 2.1.28 (Strong approximation of Nédélec elements 2). *There exists an interpolation operator $\boldsymbol{\Pi}^h : L^2(\Omega)^3 \to \boldsymbol{V}^h$ that satisfies the conditions of Assumption* 2.1.20 *for some $s_0 > 0$.*

Proof. It has been shown in [27] that there exists an interpolation operator $\boldsymbol{\Pi}^h : L^2(\Omega)^3 \to \boldsymbol{V}^h$ with $\|\boldsymbol{\Pi}^h \boldsymbol{v}\|_{L^2(\Omega)^3} \leq C \|\boldsymbol{v}\|_{L^2(\Omega)^3}$, $\|\boldsymbol{v} - \boldsymbol{\Pi}^h \boldsymbol{v}\|_{L^2(\Omega)^3} \leq C \|\boldsymbol{v}\|_{H(\mathrm{curl},\Omega)}$ and $\|\boldsymbol{v} - \boldsymbol{\Pi}^h \boldsymbol{v}\|_{L^2(\Omega)^3} \leq C h \|\boldsymbol{v}\|_{H^1(\mathrm{curl},\Omega)}$. By space interpolation [8, Ch. 14.2] we thus get $\|\boldsymbol{v} - \boldsymbol{\Pi}^h \boldsymbol{v}\|_{L^2(\Omega)^3} \leq C h^s \|\boldsymbol{v}\|_{H^s(\mathrm{curl},\Omega)}$ for $s \in (0,1)$ and $h := \max\{h_T : T \in \mathcal{T}\}$. □

Theorem 2.1.29 (Strong approximation of Nédélec elements 3). *Assume that Ω is decomposed into two disjoint connected subsets Ω_1, Ω_2 and $\mathcal{T}$ is a decomposition of Ω with either $T \subset \Omega_1$ or $T \subset \Omega_2$ for all $T \in \mathcal{T}$. Assume that $\boldsymbol{v}$ is in $H^{(r,r-1/2)}(\Omega_1)^3 \cap H^{(r,r-1/2)}(\Omega_2)^3$. Then Assumption 2.1.20 holds true with a set ω_T that is either in Ω_1 or Ω_2 in both cases* [6, p. 1286].

Proof. Both interpolation operators in Theorems 2.1.27 and 2.1.28 allow local estimates where there is the freedom to choose ω_T as required in the given situation. □

Theorem 2.1.30 (Eigenvalue approximation in a periodic domain). *Assume that ε_{r} is piecewise constant and two-valued on a decomposition of $\Omega := [0,1]^3$ and $\mathcal{T}$ be a discretisation, both as in Theorem* 2.1.29. *If we discretise the electric or magnetic eigenvalue problem* (1.17), (1.16) *by Nédélec edge elements, the discrete eigenvalues will converge to the exact eigenvalues for decreasing meshsize. The convergence rate for the eigenvalues approximation will be at least* 1.

Proof. Electric field: Since Ω is convex and $\partial\Omega = \emptyset$ we have by Remark 2.1.26 that $\boldsymbol{E}$ is piecewise in $(H^{r'})^3$ for $r' \geq 1/2$ and by Theorem 2.1.24 that $\boldsymbol{\nabla} \times \boldsymbol{E} \in H^{r''}(\Omega)^3$ for $r'' > 1/2$. The result follows since Theorems 2.1.28 and 2.1.29 pave the way to apply Theorem 2.1.16. Note that the eigenvalue convergence is twice as large as the rate for the spatial approximation.

Magnetic field: We find solutions $\boldsymbol{H} \in H^{s'}(\Omega)^3$ and $\boldsymbol{\nabla} \times \boldsymbol{H} \in H^{s''}(\Omega_1)^3 \cap H^{s''}(\Omega_2)^3$ for $s' > 1/2$, $s'' > 0$. The results follow in the same way as above from Theorem 2.1.29. □

2.1.6 Some Generalisations and Extensions

Collective compactness / Discrete compactness property

Convergence of the eigenvalues as in Theorem 2.1.12 (but without a rate) can also be obtained under the weaker condition that the family of discrete operators over a family of arbitrarily fine meshes is *collectively compact* [26, Ch. 2.3.3]. This can be reformulated in terms of a *discrete compactness property* of a family of approximation spaces [26, Ch. 7.3.2] and has been developed and used by many authors to prove convergence of different methods and elements, e. g. [22] [1] [10] [15] [5] [2, Sect. 19] and others.

H^1–conforming finite elements

Standard H^1-conforming spaces cannot be used in general, as already mentioned in Section 2.1.4, since solutions of Maxwell's equation can exhibit strong singularities. However, it was found out that formulating the divergence constraint in a weaker space than $L^2(\Omega)^3$ can cure the problem. Let Y be a Sobolev space in between $H^{-1}(\Omega)^3$ and $L^2(\Omega)^3$, $\boldsymbol{V}_h$ and Q_h be H^1-conforming finite element spaces of equal polynomial degree.

In the *Weighted Residual Method* [13] one considers $\boldsymbol{u}$ such that $\boldsymbol{\nabla}\cdot\boldsymbol{u} \in Y := \{\phi \in L^2(\Omega) : \|d^\gamma \phi\|_{L^2(\Omega)} < \infty\}$, where d a distance function from the singularities and γ some suitable positive number. One variant of the method is to seek $\boldsymbol{u}^h$ such that

$$\int_\Omega \left\{ \boldsymbol{\nabla} \times \boldsymbol{u}^h \cdot \boldsymbol{\nabla} \times \boldsymbol{v}^h + d^{2\gamma} \boldsymbol{\nabla}\cdot\boldsymbol{u}^h \boldsymbol{\nabla}\cdot\boldsymbol{v}^h + \nabla p_h \cdot \boldsymbol{v}^h \right\} = \int_\Omega \boldsymbol{f} \cdot \boldsymbol{v}^h \quad \text{for all } \boldsymbol{v}^h \in \boldsymbol{V}_h$$

$$\int_\Omega \boldsymbol{u}^h \cdot \nabla q_h = 0 \qquad \text{for all } q_h \in Q_h.$$

The $H^{-\alpha}$*-regularisation* considers $\boldsymbol{\nabla}\cdot\boldsymbol{u} \in Y := H^{-\alpha}(\Omega)$ for some $\alpha \in [1/2, 1]$ and in order to get computable expressions one uses grid-dependent norms [7]. Here we seek $\boldsymbol{u}^h$ such that

$$\int_\Omega \left\{ \boldsymbol{\nabla} \times \boldsymbol{u}^h \cdot \boldsymbol{\nabla} \times \boldsymbol{v}^h + h^{2\alpha} \boldsymbol{\nabla}\cdot\boldsymbol{u}^h \boldsymbol{\nabla}\cdot\boldsymbol{v}^h + \nabla p_h \cdot \boldsymbol{v}^h \right\} = \int_\Omega \boldsymbol{f} \cdot \boldsymbol{v}^h \quad \text{for all } \boldsymbol{v}^h \in \boldsymbol{V}_h$$

$$\int_\Omega \{ -\boldsymbol{u}^h \cdot \nabla q_h + h^{2(1-\alpha)} \nabla q_h \cdot \nabla q_h \} = 0 \qquad \text{for all } q_h \in Q_h.$$

An overview on this topic is given in [11]. Note that this theory follows also the scheme presented in Assumptions 2.1.13.

Differential forms

In the assumptions of this section we used a structural condition concerning $\boldsymbol{\nabla} Q$ and $\boldsymbol{V}$ (see Theorem 2.1.4 (proof), Theorem 2.1.8, or Assumption 2.1.20). This

comes naturally if one considers the electric and the magnetic field as differential forms. The underlying structure ("exact sequence") should also show up in the discrete spaces ("commuting diagram"). More on this topic can be found in [19] [2, Part. IV].

2.2 Calculation of the photonic band structure

by Christian Wieners

2.2.1 The parameterised periodic eigenvalue problem

We consider the Maxwell eigenvalue problem for the magnetic field for optic waves in a periodic medium in $\mathbb{R}^3$ with $\mu_r \equiv 1$ for the magnetic permeability (so that there is no magnetic induction in the medium), and assume that the electric permittivity ε_r is a periodic function on the lattice $\Gamma := \mathbb{Z}^3$ (that is, $\varepsilon_r(\boldsymbol{x}) = \varepsilon_r(\boldsymbol{x}+\boldsymbol{R})$ for all $\boldsymbol{R} \in \mathbb{Z}^3$). This eigenvalue problem has the following form: determine eigenfunctions $\boldsymbol{H}\colon \mathbb{R}^3 \longrightarrow \mathbb{C}^3$ and eigenvalues $\lambda \in \mathbb{C}$ such that

$$\begin{aligned} \boldsymbol{\nabla} \times \left(\varepsilon_r^{-1} \boldsymbol{\nabla} \times \boldsymbol{H}\right) &= \lambda \boldsymbol{H}, && \text{(2.17a)} \\ \boldsymbol{\nabla} \cdot \boldsymbol{H} &= 0, && \text{(2.17b)} \end{aligned}$$

in $\mathbb{R}^3$ (cf. Chapter 1.1.5).

Therefore, we proceed as in Chapter 1.1.7. If we take $\Omega := (0,1)^3$ to be the fundamental cell of the periodic structure, we have to find for any $\boldsymbol{k} \in \mathbb{R}^3$ a series of (quasi-periodic) eigenfunctions $\boldsymbol{H}$ that can be represented as

$$\boldsymbol{H}(\boldsymbol{x}) = \mathrm{e}^{\mathrm{i}\boldsymbol{k}\cdot\boldsymbol{x}} \widetilde{\boldsymbol{H}}(\boldsymbol{x}) \qquad \text{for all } \boldsymbol{x} \in \Omega\,, \tag{2.18}$$

where $\widetilde{\boldsymbol{H}}$ is now a periodic function in the fundamental cell Ω. The curl-operator applied to this ansatz yields

$$\boldsymbol{\nabla} \times \boldsymbol{H}(\boldsymbol{x}) = \mathrm{e}^{\mathrm{i}\boldsymbol{k}\cdot\boldsymbol{x}} \big(\boldsymbol{\nabla} \times \widetilde{\boldsymbol{H}}(\boldsymbol{x}) + \mathrm{i}\boldsymbol{k} \times \widetilde{\boldsymbol{H}}(\boldsymbol{x})\big) = e^{\mathrm{i}\boldsymbol{k}\cdot\boldsymbol{x}} \boldsymbol{\nabla}_{\boldsymbol{k}} \times \widetilde{\boldsymbol{H}}(\boldsymbol{x})\,.$$

Here, we have introduced the *shifted gradient operator*

$$\boldsymbol{\nabla}_{\boldsymbol{k}} = \boldsymbol{\nabla} + \mathrm{i}\boldsymbol{k} \tag{2.19}$$

and we consider the transformed eigenvalue problem: determine periodic eigenfunctions $\widetilde{\boldsymbol{H}}\colon \Omega \longrightarrow \mathbb{C}^3$ and eigenvalues $\lambda \in \mathbb{C}$ satisfying

$$\begin{aligned} \boldsymbol{\nabla}_{\boldsymbol{k}} \times \left(\varepsilon_r^{-1} \boldsymbol{\nabla}_{\boldsymbol{k}} \times \widetilde{\boldsymbol{H}}\right) &= \lambda \widetilde{\boldsymbol{H}}, && \text{(2.20a)} \\ \boldsymbol{\nabla}_{\boldsymbol{k}} \cdot \widetilde{\boldsymbol{H}} &= 0 && \text{(2.20b)} \end{aligned}$$

in Ω. Then, defining $\boldsymbol{H}$ by (2.18) indeed gives an eigenfunction of (2.17).

We recall (Theorem 2.1.7) that the spectrum is real and discrete with ordered real eigenvalues

$$0 \le \lambda_{\boldsymbol{k}}^1 \le \lambda_{\boldsymbol{k}}^2 \le \cdots \le \lambda_{\boldsymbol{k}}^N \le \cdots .$$

The Floquet–Bloch theory guarantees that the full spectrum of the Maxwell operator associated to problem (2.17) can be computed by a series of eigenvalue problems (2.20) in the fundamental cell $\Omega = (0,1)^3$ of the periodic structure, where it is sufficient that $\boldsymbol{k}$ is in the Brillouin zone $B = [-\pi, \pi]^3$. The spectrum of the problem (2.17) is given by

$$\sigma = \bigcup_{n\in\mathbb{N}} [\inf_{\boldsymbol{k}\in B} \lambda_{\boldsymbol{k}}^n, \sup_{\boldsymbol{k}\in B} \lambda_{\boldsymbol{k}}^n]$$

and possible nonempty intervals

$$(\sup_{\boldsymbol{k}\in B} \lambda_{\boldsymbol{k}}^n, \inf_{\boldsymbol{k}\in B} \lambda_{\boldsymbol{k}}^{n+1})$$

are called band gaps. In the following we develop a numerical method to compute photonic bandstructures to find such bandgaps.

2.2.2 Galerkin approximation of the eigenvalue problems

In the next step, we derive a weak formulation for the eigenvalue problem (2.20). This allows for general coefficients $\varepsilon_{\mathrm{r}} \in L^\infty(\Omega)$ with $1 \le \varepsilon_{\mathrm{r}}(\boldsymbol{x}) \le \varepsilon_\infty$ for almost all $\boldsymbol{x} \in \Omega$. In principle, it is also possible to consider a tensor-valued electric permittivity ε_{r} (as it is required, e. g., for anisotropic materials), but in our examples we will consider only the special case that we have a material with $\varepsilon_\infty > 1$ in a subset $\omega \subset \Omega$ and empty space in $\Omega \setminus \omega$, where we set $\varepsilon_{\mathrm{r}} = 1$.

We use the spaces

$$\begin{aligned} \boldsymbol{V} &= H_{\mathrm{per}}(\mathrm{curl}, \Omega) := \left\{ \boldsymbol{u}|_\Omega \colon \boldsymbol{u} \in H(\mathrm{curl}, \mathbb{R}^3/\mathbb{Z}^3) \right\}, \\ Q &= H^1_{\mathrm{per}}(\Omega) := \left\{ q|_\Omega \colon q \in H^1(\mathbb{R}^3/\mathbb{Z}^3) \right\} \end{aligned}$$

of periodic functions on $\Omega = (0,1)^3$ (that is, with periodic boundary conditions on $\partial\Omega$ for the corresponding trace operator), see Chapter 1.2.6. For $\boldsymbol{u}, \boldsymbol{v} \in \boldsymbol{V}$ and $p, q \in Q$ we define the Hermitian sesqui-linear forms[1]

$$\begin{aligned} a_{\boldsymbol{k}}(\boldsymbol{u}, \boldsymbol{v}) &= \int_\Omega \varepsilon_{\mathrm{r}}^{-1} \overline{\boldsymbol{\nabla}_{\boldsymbol{k}} \times \boldsymbol{u}} \cdot \boldsymbol{\nabla}_{\boldsymbol{k}} \times \boldsymbol{v} \, dx \,, \\ m(\boldsymbol{u}, \boldsymbol{v}) &= \int_\Omega \overline{\boldsymbol{u}} \cdot \boldsymbol{v} \, dx \,, \end{aligned}$$

[1] Note that in our notation the sesqui-linear forms (and also all dual pairings) are anti-linear in the first component.

$$b_{\boldsymbol{k}}(\boldsymbol{v}, q) = \int_\Omega \overline{\boldsymbol{v}} \cdot \boldsymbol{\nabla}_{\boldsymbol{k}} q \, dx \,,$$
$$c_{\boldsymbol{k}}(p, q) = \int_\Omega \overline{\boldsymbol{\nabla}_{\boldsymbol{k}} p} \cdot \boldsymbol{\nabla}_{\boldsymbol{k}} q \, dx \,,$$

and we define — depending on the Floquet parameter $\boldsymbol{k}$ — the subspace which includes the $\boldsymbol{k}$-divergence constraint (2.20b) by

$$\boldsymbol{X}_{\boldsymbol{k}} \quad = \big\{ \boldsymbol{v} \in \boldsymbol{V} \colon b_{\boldsymbol{k}}(\boldsymbol{v}, q) = 0 \text{ for all } q \in Q \big\}$$

($\boldsymbol{X}_{\boldsymbol{0}} = \boldsymbol{V}_1$ in (2.7)). Now, we can rewrite the equation (2.20) in weak form: find $(\boldsymbol{u}, \lambda) \in \boldsymbol{X}_{\boldsymbol{k}} \setminus \{0\} \times \mathbb{R}$ such that

$$a_{\boldsymbol{k}}(\boldsymbol{u}, \boldsymbol{v}) = \lambda \, m(\boldsymbol{u}, \boldsymbol{v}) \qquad \text{for all } \boldsymbol{v} \in \boldsymbol{X}_{\boldsymbol{k}} \,. \tag{2.21}$$

Obviously, $\boldsymbol{\nabla}_{\boldsymbol{k}} Q$ is contained in the kernel of the sesqui-linear form $a_{\boldsymbol{k}}(\cdot, \cdot)$, i. e., $a_{\boldsymbol{k}}(\boldsymbol{v}, \boldsymbol{v}) = 0$ for $\boldsymbol{v} = \boldsymbol{\nabla}_{\boldsymbol{k}} q$ with $q \in Q$. Moreover, for any $\delta > 0$, the sesqui-linear form

$$a^\delta_{\boldsymbol{k}}(\boldsymbol{u}, \boldsymbol{v}) = a_{\boldsymbol{k}}(\boldsymbol{u}, \boldsymbol{v}) + \delta \, m(\boldsymbol{u}, \boldsymbol{v}) \tag{2.22}$$

is elliptic in $\boldsymbol{V}$ (and thus also in $\boldsymbol{X}_{\boldsymbol{k}}$). Since $\boldsymbol{X}_{\boldsymbol{k}}$ embeds compactly into $L^2_{\mathrm{per}}(\Omega)^3$ (see Theorem 1.2.1 and Theorem 2.1.7), the spectrum of the corresponding self-adjoint operator is discrete, positive, and all eigenvalues have finite multiplicity. As a consequence, the eigenvalue problem (2.21) has a discrete non-negative spectrum, and the dimension of kernel of the sesqui-linear form $a_{\boldsymbol{k}}(\cdot, \cdot)$ in $\boldsymbol{X}_{\boldsymbol{k}}$ is finite.

For the discrete Galerkin approximation of (2.21) we consider finite element subspaces $\boldsymbol{V}_{h,\boldsymbol{k}} \subset \boldsymbol{V}$ and $Q_{h,\boldsymbol{k}} \subset Q$, and we define the constrained discrete space

$$\boldsymbol{X}_{h,\boldsymbol{k}} \quad = \quad \{ \boldsymbol{v}_h \in \boldsymbol{V}_h \colon b_{\boldsymbol{k}}(\boldsymbol{v}_h, q_h) = 0 \text{ for all } q_h \in Q_h \} \,.$$

Note that in $\boldsymbol{X}_{h,\boldsymbol{k}}$ the $\boldsymbol{k}$-divergence constraint is fulfilled only approximately, so that the discretisation is non-conforming, i. e., we have $\boldsymbol{X}_{h,\boldsymbol{k}} \not\subset \boldsymbol{X}_{\boldsymbol{k}}$.

On the discrete space, we define the Galerkin approximation:
find $(\boldsymbol{u}_{h,\boldsymbol{k}}, \lambda_{h,\boldsymbol{k}}) \in \boldsymbol{X}_{h,\boldsymbol{k}} \setminus \{0\} \times \mathbb{R}$ such that

$$a_{\boldsymbol{k}}(\boldsymbol{u}_{h,\boldsymbol{k}}, \boldsymbol{v}_{h,\boldsymbol{k}}) = \lambda_{h,\boldsymbol{k}} \, m(\boldsymbol{u}_{h,\boldsymbol{k}}, \boldsymbol{v}_{h,\boldsymbol{k}}) \qquad \text{for all } \boldsymbol{v}_{h,\boldsymbol{k}} \in \boldsymbol{X}_{h,\boldsymbol{k}} \,. \tag{2.23}$$

Due to the nonconformity of the discretisation, it is not a priori clear that all eigenvalues of the discrete problem indeed approximate the eigenvalues of the continuous problem, compare Chapter 2.1.4. This requires a suitable choice of the finite element spaces.

For the numerical analysis of the eigenvalue problem (2.23) we refer to [4]. If the Assumptions 2.1.13 and 2.1.20 can be verified (as in the previous section for $\boldsymbol{k} = \boldsymbol{0}$), we can apply Theorem 2.1.16 which guarantees eigenvalue convergence.

2.2.3 Lowest order conforming finite elements on hexahedral meshes

We now introduce a family of finite element spaces which satisfy the required conditions for eigenvalue convergence [4].

Let $\bar{\Omega} = \cup_{c\in\mathcal{C}_h}\bar{\Omega}_c$ be a decomposition into hexahedral cells $c \in \mathcal{C}_h$, and let $\varphi_c\colon \hat{\Omega} = [0,1]^3 \longrightarrow \Omega_c$ be the transformation to the reference cell. For $\boldsymbol{k} = \mathbf{0}$ we use the standard Nédélec elements with edge degrees of freedom [26, Chap. 6.3] and standard trilinear conforming H^1 elements, i. e.,

$$\begin{aligned}\boldsymbol{V}_{h,\mathbf{0}} &= \{\boldsymbol{u} \in \boldsymbol{X}_{\mathbf{0}}\colon D\varphi_c^T\boldsymbol{u}\circ\varphi_c \in \mathcal{P}_{0,1,1}\boldsymbol{e}_x + \mathcal{P}_{1,0,1}\boldsymbol{e}_y + \mathcal{P}_{1,1,0}\boldsymbol{e}_z \text{ for all } c\in\mathcal{C}_h\},\\ Q_{h,\mathbf{0}} &= \{q \in Q\colon q\circ\varphi_c \in \mathcal{P}_{1,1,1} \text{ for all } c\in\mathcal{C}_h\}\,,\end{aligned}$$

where $\mathcal{P}_{i,j,k}$ denotes the space of polynomials with degree i,j,k in coordinate x_1, x_2, x_3, respectively. For the implementation we use a nodal basis in both cases, where each basis function is associated to a nodal point.

Let $\{\boldsymbol{z}_v\colon v \in \mathcal{V}_h\} \subset \bar{\Omega}$ be the set of all vertices, where $\mathcal{V}_h$ denotes an index set enumerating the vertices, and let $\mathcal{E}_h$ be the set of all edges $e = (\boldsymbol{x}_e, \boldsymbol{y}_e)$, i. e., e is understood as an ordered tupel of two vertices. Note that this defines an orientation for every edge which is independent of the cells. The midpoint of e is defined by $\boldsymbol{z}_e = (\boldsymbol{x}_e + \boldsymbol{y}_e)/2$ and and its tangent by $\boldsymbol{t}_e = \boldsymbol{y}_e - \boldsymbol{x}_e$.

In $\boldsymbol{V}_{h,\mathbf{0}}$ a nodal basis function $\boldsymbol{\psi}_{e,\mathbf{0}}$ is associated to every edge $e \in \mathcal{E}_h$ such that for all $\boldsymbol{u}_{h,\mathbf{0}} \in \boldsymbol{V}_{h,\mathbf{0}}$

$$\boldsymbol{u}_{h,\mathbf{0}} = \sum_{e\in\mathcal{E}_h}\langle\boldsymbol{\psi}'_{e,\mathbf{0}}, \boldsymbol{u}_{h,\mathbf{0}}\rangle\boldsymbol{\psi}_{e,\mathbf{0}}\,, \qquad \langle\boldsymbol{\psi}'_{e,\mathbf{0}}, \boldsymbol{u}_{h,\mathbf{0}}\rangle = \int_{\boldsymbol{x}_e}^{\boldsymbol{y}_e}\boldsymbol{u}_{h,\mathbf{0}}\cdot\boldsymbol{t}_e\,ds\,.$$

Here, the dual functionals $\boldsymbol{\psi}'_{e,\mathbf{0}} \in \boldsymbol{V}'_{h,\mathbf{0}}$ denote the degree of freedom associated to the edge e. Note that due to the periodic boundary conditions the boundary degrees of freedom are not independent, i. e., we have $\boldsymbol{\psi}'_{e_1,\mathbf{0}} = \boldsymbol{\psi}'_{e_2,\mathbf{0}}$ if $\boldsymbol{z}_{e_1}, \boldsymbol{z}_{e_2} \in \partial\Omega$ with $\boldsymbol{z}_{e_1} - \boldsymbol{z}_{e_2} \in \mathbb{Z}^3$.

Analogously, we have nodal basis functions $\phi_{v,\mathbf{0}} \in Q_{h,\mathbf{0}}$ associated to a vertex v such that for all $q_{h,\mathbf{0}} \in Q_{h,\mathbf{0}}$

$$q_{h,\mathbf{0}} = \sum_{v\in\mathcal{V}_h}\langle\phi'_{v,\mathbf{0}}, q_{h,\mathbf{0}}\rangle\phi_{v,\mathbf{0}}\,, \qquad \langle\phi'_{v,\mathbf{0}}, q_{h,\mathbf{0}}\rangle = q_{h,\mathbf{0}}(\boldsymbol{z}_v)\,.$$

Again, the degrees of freedom $\phi'_{v,\mathbf{0}} \in Q_{h,\mathbf{0}}$ are periodic, i. e., $\phi'_{v_1,\mathbf{0}} = \phi'_{v_2,\mathbf{0}}$ and thus $q_{h,\mathbf{0}}(\boldsymbol{z}_{v_1}) = q_{h,\mathbf{0}}(\boldsymbol{z}_{v_2})$ for $\boldsymbol{z}_{v_1}, \boldsymbol{z}_{v_2} \in \partial\Omega$ with $\boldsymbol{z}_{v_1} - \boldsymbol{z}_{v_2} \in \mathbb{Z}^3$.

An important feature of the pair of finite element spaces $\boldsymbol{V}_{h,\mathbf{0}} \times Q_{h,\mathbf{0}}$ is the property $\boldsymbol{\nabla}Q_{h,\mathbf{0}} \subset \boldsymbol{V}_{h,\mathbf{0}}$ (see Theorem 2.1.8), i. e., we have

$$\boldsymbol{\nabla}q_{h,\mathbf{0}} \quad = \quad \sum_{e\in\mathcal{E}_h}\langle\boldsymbol{\psi}'_{e,\mathbf{0}}, \boldsymbol{\nabla}q_{h,\mathbf{0}}\rangle\boldsymbol{\psi}_{e,\mathbf{0}} \tag{2.24}$$

for all $q_{h,\mathbf{0}} \in Q_{h,\mathbf{0}}$.

2.2.4 Conforming elements with phase-shifted nodal basis

Starting from the standard nodal basis and degrees of freedom, we now consider modified elements for $\boldsymbol{k} \neq \boldsymbol{0}$ with a *phase shift*: we define

$$\begin{aligned} \boldsymbol{V}_{h,\boldsymbol{k}} &= \operatorname{Span}\{\boldsymbol{\psi}_{e,\boldsymbol{k}} \colon e \in \mathcal{E}_h\}, \qquad \boldsymbol{\psi}_{e,\boldsymbol{k}}(\boldsymbol{x}) = \mathrm{e}^{-\mathrm{i}\boldsymbol{k}\cdot(\boldsymbol{x}-\boldsymbol{z}_e)}\boldsymbol{\psi}_{e,\boldsymbol{0}}(\boldsymbol{x})\,, \\ Q_{h,\boldsymbol{k}} &= \operatorname{Span}\{\phi_{v,\boldsymbol{k}} \colon v \in \mathcal{V}_h\}, \qquad \phi_{v,\boldsymbol{k}}(\boldsymbol{x}) = \mathrm{e}^{-\mathrm{i}\boldsymbol{k}\cdot(\boldsymbol{x}-\boldsymbol{z}_v)}\phi_{v,\boldsymbol{0}}(\boldsymbol{x}) \end{aligned}$$

with the basis representation depending on the phase-shifted degrees of freedom

$$\begin{aligned} \boldsymbol{u}_{h,\boldsymbol{k}} &= \sum_{e\in\mathcal{E}_h} \langle \boldsymbol{\psi}'_{e,\boldsymbol{k}}, \boldsymbol{u}_{h,\boldsymbol{k}}\rangle \boldsymbol{\psi}_{e,\boldsymbol{k}}\,, \qquad \langle \boldsymbol{\psi}'_{e,\boldsymbol{k}}, \boldsymbol{u}_{h,\boldsymbol{k}}\rangle = \int_{\boldsymbol{x}_e}^{\boldsymbol{y}_e} \mathrm{e}^{\mathrm{i}\boldsymbol{k}\cdot(\boldsymbol{x}-\boldsymbol{z}_e)}\boldsymbol{u}_{h,\boldsymbol{0}}\cdot\boldsymbol{t}_e\,ds\,, \\ q_{h,\boldsymbol{k}} &= \sum_{v\in\mathcal{V}_h} \langle \phi'_{v,\boldsymbol{k}}, q_{h,\boldsymbol{k}}\rangle \phi_{v,\boldsymbol{k}}\,, \qquad \langle \phi'_{v,\boldsymbol{k}}, q_{h,\boldsymbol{0}}\rangle = q_{h,\boldsymbol{k}}(\boldsymbol{z}_v)\,. \end{aligned}$$

In the implementation we use the transformation properties of the phase-shifted basis functions: we have

$$\begin{aligned} \boldsymbol{\nabla}_{\boldsymbol{k}}\,\phi_{v,\boldsymbol{k}}(\boldsymbol{x}) &= \mathrm{e}^{-\mathrm{i}\boldsymbol{k}\cdot(\boldsymbol{x}-\boldsymbol{z}_v)}\boldsymbol{\nabla}\phi_{v,\boldsymbol{0}}(\boldsymbol{x})\,, \\ \boldsymbol{\nabla}_{\boldsymbol{k}}\times\boldsymbol{\psi}_{e,\boldsymbol{k}}(\boldsymbol{x}) &= \mathrm{e}^{-\mathrm{i}\boldsymbol{k}\cdot(\boldsymbol{x}-\boldsymbol{z}_e)}\boldsymbol{\nabla}\times\boldsymbol{\psi}_{e,\boldsymbol{0}}(\boldsymbol{x})\,, \\ \boldsymbol{\nabla}_{\boldsymbol{k}}\cdot\boldsymbol{\psi}_{e,\boldsymbol{k}}(\boldsymbol{x}) &= \mathrm{e}^{-\mathrm{i}\boldsymbol{k}\cdot(\boldsymbol{x}-\boldsymbol{z}_e)}\boldsymbol{\nabla}\cdot\boldsymbol{\psi}_{e,\boldsymbol{0}}(\boldsymbol{x})\,. \end{aligned}$$

As a consequence, all sesqui-linear forms are obtained by simple scaling, i. e.,

$$\begin{aligned} a_{\boldsymbol{k}}(\boldsymbol{\psi}_{e_1,\boldsymbol{k}}, \boldsymbol{\psi}_{e_2,\boldsymbol{k}}) &= \mathrm{e}^{-\mathrm{i}\boldsymbol{k}\cdot(\boldsymbol{z}_{e_1}-\boldsymbol{z}_{e_2})}\, a_{\boldsymbol{0}}(\boldsymbol{\psi}_{e_1,\boldsymbol{0}}, \boldsymbol{\psi}_{e_2,\boldsymbol{0}}), \\ m(\boldsymbol{\psi}_{e_1,\boldsymbol{k}}, \boldsymbol{\psi}_{e_2,\boldsymbol{k}}) &= \mathrm{e}^{-\mathrm{i}\boldsymbol{k}\cdot(\boldsymbol{z}_{e_1}-\boldsymbol{z}_{e_2})}\, m(\boldsymbol{\psi}_{e_1,\boldsymbol{0}}, \boldsymbol{\psi}_{e_2,\boldsymbol{0}}), \\ b_{\boldsymbol{k}}(\boldsymbol{\psi}_{e,\boldsymbol{k}}, \phi_{v,\boldsymbol{k}}) &= \mathrm{e}^{-\mathrm{i}\boldsymbol{k}\cdot(\boldsymbol{z}_e-\boldsymbol{z}_v)}\, b_{\boldsymbol{0}}(\boldsymbol{\psi}_{e,\boldsymbol{0}}, \phi_{v,\boldsymbol{0}}), \\ c_{\boldsymbol{k}}(\phi_{v_1,\boldsymbol{k}}, \phi_{v_2,\boldsymbol{k}}) &= \mathrm{e}^{-\mathrm{i}\boldsymbol{k}\cdot(\boldsymbol{z}_{v_1}-\boldsymbol{z}_{v_2})}\, c_{\boldsymbol{0}}(\phi_{v_1,\boldsymbol{0}}, \phi_{v_2,\boldsymbol{0}}) \end{aligned}$$

for all $e, e_1, e_2 \in \mathcal{E}_h$ and $v, v_1, v_2 \in \mathcal{V}_h$. This property makes the use of the phase-shifted basis very attractive, and only small modifications from the standard elements are required in the implementation. In particular, inserting (2.24) we obtain

$$\begin{aligned} \boldsymbol{\nabla}_{\boldsymbol{k}}\,\phi_{v,\boldsymbol{k}}(\boldsymbol{x}) &= \mathrm{e}^{-\mathrm{i}\boldsymbol{k}\cdot(\boldsymbol{x}-\boldsymbol{z}_v)}\boldsymbol{\nabla}\phi_{v,\boldsymbol{0}}(\boldsymbol{x}) \\ &= \mathrm{e}^{-\mathrm{i}\boldsymbol{k}\cdot(\boldsymbol{x}-\boldsymbol{z}_v)} \sum_{e\in\mathcal{E}_h} \langle \boldsymbol{\psi}'_{e,\boldsymbol{0}}, \boldsymbol{\nabla}\phi_{v,\boldsymbol{0}}\rangle \boldsymbol{\psi}_{e,\boldsymbol{0}}(\boldsymbol{x}) \\ &= \mathrm{e}^{\mathrm{i}\boldsymbol{k}\cdot\boldsymbol{z}_v} \sum_{e\in\mathcal{E}_h} \langle \boldsymbol{\psi}'_{e,\boldsymbol{k}}, \boldsymbol{\nabla}\phi_{v,\boldsymbol{0}}\rangle \mathrm{e}^{-\mathrm{i}\boldsymbol{k}\cdot\boldsymbol{z}_e}\boldsymbol{\psi}_{e,\boldsymbol{k}}(\boldsymbol{x})\,, \end{aligned}$$

i. e., the inclusion $\boldsymbol{\nabla}_{\boldsymbol{k}} Q_{h,\boldsymbol{k}} \subset \boldsymbol{V}_{h,\boldsymbol{k}}$ is also satisfied for the phase-shifted elements.

The sesqui-linear form $c_{\boldsymbol{0}}(\cdot,\cdot)$ vanishes for all constants, i. e., $c_{\boldsymbol{0}}(\boldsymbol{v},\boldsymbol{v}) = 0$ if and only if $\boldsymbol{v}$ is constant. Thus, $c_{\boldsymbol{0}}(\cdot,\cdot)$ is elliptic in $\hat{Q}_{h,\boldsymbol{0}} = Q_{h,\boldsymbol{0}}/\mathbb{R}$. For $\boldsymbol{k} \neq \boldsymbol{0}$ we observe that the sesqui-linear form $c_{\boldsymbol{k}}(\cdot,\cdot)$ is elliptic in $Q_{h,\boldsymbol{k}}$, since the kernel of the operator $\boldsymbol{\nabla}_{\boldsymbol{k}}$ is spanned by non-periodic functions $\mathrm{e}^{i\boldsymbol{k}\cdot\boldsymbol{x}}$. For $\boldsymbol{k} \neq \boldsymbol{0}$ we set $\hat{Q}_{h,\boldsymbol{k}} = Q_{h,\boldsymbol{k}}$ in order to unify the notation.

2.2.5 Discrete operators

For the formulation of the following algorithms we introduce discrete operators

$$\begin{aligned} A_{h,\boldsymbol{k}} &: \boldsymbol{V}_{h,\boldsymbol{k}} \longrightarrow \boldsymbol{V}'_{h,\boldsymbol{k}}\,, \\ M_{h,\boldsymbol{k}} &: \boldsymbol{V}_{h,\boldsymbol{k}} \longrightarrow \boldsymbol{V}'_{h,\boldsymbol{k}}\,, \\ B_{h,\boldsymbol{k}} &: \boldsymbol{V}_{h,\boldsymbol{k}} \longrightarrow Q'_{h,\boldsymbol{k}}\,, \\ C_{h,\boldsymbol{k}} &: Q_{h,\boldsymbol{k}} \longrightarrow Q'_{h,\boldsymbol{k}} \end{aligned}$$

induced by the sesqui-linear forms, i. e.,

$$\begin{aligned} \langle A_{h,\boldsymbol{k}}\boldsymbol{\psi}_{e_1,\boldsymbol{k}}, \boldsymbol{\psi}_{e_2,\boldsymbol{k}}\rangle &= a_{\boldsymbol{k}}(\boldsymbol{\psi}_{e_1,\boldsymbol{k}}, \boldsymbol{\psi}_{e_2,\boldsymbol{k}})\,, \\ \langle M_{h,\boldsymbol{k}}\boldsymbol{\psi}_{e_1,\boldsymbol{k}}, \boldsymbol{\psi}_{e_2,\boldsymbol{k}}\rangle &= m(\boldsymbol{\psi}_{e_1,\boldsymbol{k}}, \boldsymbol{\psi}_{e_2,\boldsymbol{k}})\,, \\ \langle B_{h,\boldsymbol{k}}\boldsymbol{\psi}_{e,\boldsymbol{k}}, \phi_{v,\boldsymbol{k}}\rangle &= b_{\boldsymbol{k}}(\boldsymbol{\psi}_{e,\boldsymbol{k}}, \phi_{v,\boldsymbol{k}})\,, \\ \langle C_{h,\boldsymbol{k}}\phi_{v_1,\boldsymbol{k}}, \phi_{v_2,\boldsymbol{k}}\rangle &= c_{\boldsymbol{k}}(\phi_{v_1,\boldsymbol{k}}, \phi_{v_2,\boldsymbol{k}}) \end{aligned}$$

for all $e, e_1, e_2 \in \mathcal{E}_h$ and $v, v_1, v_2 \in \mathcal{V}_h$. In the implementation, the operators are represented by matrices $\underline{A}_{h,\boldsymbol{k}} = \big(\underline{A}_{e_1,e_2}\big)_{e_1,e_2\in\mathcal{E}_h}$, $\underline{M}_{h,\boldsymbol{k}} = \big(\underline{M}_{e_1,e_2}\big)_{e_1,e_2\in\mathcal{E}_h}$, $\underline{B}_{h,\boldsymbol{k}} = \big(\underline{B}_{v,e}\big)_{v\in\mathcal{V}_h,e\in\mathcal{E}_h}$, $\underline{C}_{h,\boldsymbol{k}} = \big(\underline{C}_{v_1,v_2}\big)_{v_1,v_2\in\mathcal{V}_h}$ with

$$\begin{aligned} A_{h,\boldsymbol{k}} &= \sum_{e_1,e_2\in\mathcal{E}_h} \underline{A}_{e_1,e_2}\boldsymbol{\psi}'_{e_2,\boldsymbol{k}} \otimes \boldsymbol{\psi}'_{e_1,\boldsymbol{k}}\,, & \underline{A}_{e_1,e_2} &= a_{\boldsymbol{k}}(\boldsymbol{\psi}_{e_2,\boldsymbol{k}}, \boldsymbol{\psi}_{e_1,\boldsymbol{k}})\,, \\ M_{h,\boldsymbol{k}} &= \sum_{e_1,e_2\in\mathcal{E}_h} \underline{M}_{e_1,e_2}\boldsymbol{\psi}'_{e_2,\boldsymbol{k}} \otimes \boldsymbol{\psi}'_{e_1,\boldsymbol{k}}\,, & \underline{M}_{e_1,e_2} &= m(\boldsymbol{\psi}_{e_2,\boldsymbol{k}}, \boldsymbol{\psi}_{e_1,\boldsymbol{k}})\,, \\ B_{h,\boldsymbol{k}} &= \sum_{v\in\mathcal{V}_h,e\in\mathcal{E}_h} \underline{B}_{v,e}\boldsymbol{\psi}'_{e,\boldsymbol{k}} \otimes \phi'_{v,\boldsymbol{k}}\,, & \underline{B}_{v,e} &= b_{\boldsymbol{k}}(\boldsymbol{\psi}_{e,\boldsymbol{k}}, \phi_{v,\boldsymbol{k}})\,, \\ C_{h,\boldsymbol{k}} &= \sum_{v_1,v_2\in\mathcal{V}_h} \underline{C}_{v_1,v_2}\phi'_{v_2,\boldsymbol{k}} \otimes \phi'_{v_1,\boldsymbol{k}}\,, & \underline{C}_{v_1,v_2} &= c_{\boldsymbol{k}}(\phi_{v_2,\boldsymbol{k}}, \phi_{v_1,\boldsymbol{k}})\,, \end{aligned}$$

where the rank-one-operators are defined by $(\boldsymbol{\psi}'_1 \otimes \boldsymbol{\psi}'_2)\boldsymbol{u} = \langle \boldsymbol{\psi}'_1, \boldsymbol{u}\rangle\, \boldsymbol{\psi}'_2$. In all cases, the matrix representation is sparse, i. e., the number of non-zero entries is proportional to the number of edges and vertices. The matrix representations of $A_{h,\boldsymbol{k}}$ and $C_{h,\boldsymbol{k}}$ are used in the construction of smoothers for the multigrid iteration. A matrix representation of $B_{h,\boldsymbol{k}}$ can be avoided in the implementation since the operator can be directly evaluated by

$$B_{h,\boldsymbol{k}}\boldsymbol{v}_{h,\boldsymbol{k}} = \sum_{v\in\mathcal{V}_h} b_{\boldsymbol{k}}(\boldsymbol{v}_{h,\boldsymbol{k}}, \phi_{v,\boldsymbol{k}})\phi'_{v,\boldsymbol{k}}$$

and the coefficients can be computed by local integration. Nevertheless, using a matrix representation is far more efficient since this operation is applied very often.

The operator $B_{h,\boldsymbol{k}}\colon \boldsymbol{V}_{h,\boldsymbol{k}} \longrightarrow Q'_{h,\boldsymbol{k}}$ is the phase-shifted divergence operator in weak form, and its adjoint $B'_{h,\boldsymbol{k}}\colon Q_{h,\boldsymbol{k}} \longrightarrow \boldsymbol{V}'_{h,\boldsymbol{k}}$ corresponds to the weak phase-shifted gradient. It is an important observation for our algorithms, that the strong

consistency property $\boldsymbol{\nabla}_{\boldsymbol{k}} Q_{h,\boldsymbol{k}} \subset \boldsymbol{V}_{h,\boldsymbol{k}}$ of the discretisations allows also for a phase-shifted gradient operator in strong form

$$S_{h,\boldsymbol{k}} \colon Q_{h,\boldsymbol{k}} \longrightarrow \boldsymbol{V}_{h,\boldsymbol{k}}$$

which is defined by nodal evaluation, i. e.,

$$\begin{aligned} S_{h,\boldsymbol{k}} q_{h,\boldsymbol{k}} &= \sum_{e \in \mathcal{E}_h} \langle \boldsymbol{\psi}'_{e,\boldsymbol{k}}, \boldsymbol{\nabla}_{\boldsymbol{k}} q_{h,\boldsymbol{k}} \rangle \boldsymbol{\psi}_{e,\boldsymbol{k}} \\ &= \sum_{e=(\boldsymbol{x}_e,\boldsymbol{y}_e) \in \mathcal{E}_h} \Big(q_{h,\boldsymbol{k}}(\boldsymbol{y}_e) \mathrm{e}^{\mathrm{i}\boldsymbol{k}\cdot(\boldsymbol{y}_e - \boldsymbol{z}_e)} - q_{h,\boldsymbol{k}}(\boldsymbol{x}_e) \mathrm{e}^{\mathrm{i}\boldsymbol{k}\cdot(\boldsymbol{x}_e - \boldsymbol{z}_e)} \Big) \boldsymbol{\psi}_{e,\boldsymbol{k}} \,. \end{aligned}$$

corresponding to the matrix representation $\underline{S}_{h,\boldsymbol{k}} = \big(\underline{S}_{e,v}\big)_{e \in \mathcal{E}_h, v \in \mathcal{V}_h}$ with

$$S_{h,\boldsymbol{k}} = \sum_{e \in \mathcal{E}_h,\, v \in \mathcal{V}_h} \underline{S}_{e,v} \phi'_{v,\boldsymbol{k}} \otimes \boldsymbol{\psi}_{e,\boldsymbol{k}} \,, \quad \underline{S}_{e,v} = \phi_{v,\boldsymbol{k}}(\boldsymbol{y}_e) \mathrm{e}^{\mathrm{i}\boldsymbol{k}\cdot(\boldsymbol{y}_e - \boldsymbol{z}_e)} - \phi_{v,\boldsymbol{k}}(\boldsymbol{x}_e) \mathrm{e}^{\mathrm{i}\boldsymbol{k}\cdot(\boldsymbol{x}_e - \boldsymbol{z}_e)} .$$

Moreover, this operator satisfies the compatibility condition

$$b_{\boldsymbol{k}}(S_{h,\boldsymbol{k}} p_{h,\boldsymbol{k}}, q_{h,\boldsymbol{k}}) = c_{\boldsymbol{k}}(p_{h,\boldsymbol{k}}, q_{h,\boldsymbol{k}}) \,,$$

i. e., the operator equation $B_{h,\boldsymbol{k}} S_{h,\boldsymbol{k}} = C_{h,\boldsymbol{k}}$.

A direct consequence of this compatibility is the inf-sup stability of the finite element pair $\boldsymbol{V}_{h,\boldsymbol{k}} \times \hat{Q}_{h,\boldsymbol{k}}$, i. e.,

$$\begin{aligned} \sup_{\boldsymbol{v}_{h,\boldsymbol{k}} \in \boldsymbol{V}_{h,\boldsymbol{k}} \setminus \{0\}} \frac{b_{\boldsymbol{k}}(\boldsymbol{v}_{h,\boldsymbol{k}}, q_{h,\boldsymbol{k}})}{\|\boldsymbol{v}_{h,\boldsymbol{k}}\|_{H(\mathrm{curl},\Omega)}} &\geq \frac{b_{\boldsymbol{k}}(S_{h,\boldsymbol{k}} q_{h,\boldsymbol{k}}, q_{h,\boldsymbol{k}})}{\|S_{h,\boldsymbol{k}} q_{h,\boldsymbol{k}}\|_{H(\mathrm{curl},\Omega)}} = \frac{c_{\boldsymbol{k}}(q_{h,\boldsymbol{k}}, q_{h,\boldsymbol{k}})}{\|S_{h,\boldsymbol{k}} q_{h,\boldsymbol{k}}\|_{L^2(\Omega,\mathbb{C}^3)}} \\ &\geq \beta \, \|q_{h,\boldsymbol{k}}\|_{H^1(\Omega,\mathbb{C}^3)} \end{aligned} \tag{2.25}$$

for all $q_{h,\boldsymbol{k}} \in \hat{Q}_{h,\boldsymbol{k}}$, where the constant $\beta > 0$ is independent of the mesh size and can be computed from the Poincaré–Friedrich constant. Recall how this is used to prove Theorem 2.1.8.

Further compatibility properties can be formulated as an exact sequence property, cf. [26, 19]. In particular, the operator $S_{h,\boldsymbol{k}}$ maps into the kernel of $A_{h,\boldsymbol{k}}$, i. e., $A_{h,\boldsymbol{k}} S_{h,\boldsymbol{k}} = 0$. In order to obtain a preconditioner for the LOBPCG method, we define the stabilised Maxwell operator $A^{\delta}_{h,\boldsymbol{k}} = A_{h,\boldsymbol{k}} + \delta M_{h,\boldsymbol{k}}$ for $\delta > 0$. This operator is self-adjoint and regular, and we will see below how to construct a robust multigrid preconditioner for this operator.

2.2.6 The projection onto the constrained space

Since for the constrained space $\boldsymbol{X}_{h,\boldsymbol{k}}$ no local basis exists, we construct approximations in the full space $\boldsymbol{V}_{h,\boldsymbol{k}}$ and we provide a projection onto $\boldsymbol{X}_{h,\boldsymbol{k}}$.

This projection can be constructed as follows: for $\boldsymbol{v}_{h,\boldsymbol{k}} \in \boldsymbol{V}_{h,\boldsymbol{k}}$ we construct $p_{h,\boldsymbol{k}} \in Q_{h,\boldsymbol{k}}$ such that $\boldsymbol{v}_{h,\boldsymbol{k}} - \boldsymbol{\nabla}_{\boldsymbol{k}} p_{h,\boldsymbol{k}} \in \boldsymbol{X}_{h,\boldsymbol{k}}$, i. e.,

$$\begin{aligned} 0 &= b_{\boldsymbol{k}}(\boldsymbol{v}_{h,\boldsymbol{k}} - \boldsymbol{\nabla}_{\boldsymbol{k}} p_{h,\boldsymbol{k}}, q_{h,\boldsymbol{k}}) \\ &= b_{\boldsymbol{k}}(\boldsymbol{v}_{h,\boldsymbol{k}}, q_{h,\boldsymbol{k}}) - c_{\boldsymbol{k}}(p_{h,\boldsymbol{k}}, q_{h,\boldsymbol{k}}) \quad \text{for all} \quad q_{h,\boldsymbol{k}} \in Q_{h,\boldsymbol{k}} \,. \end{aligned}$$

Thus, we have $B_{h,\boldsymbol{k}} \boldsymbol{v}_{h,\boldsymbol{k}} = C_{h,\boldsymbol{k}} p_{h,\boldsymbol{k}}$ and $\boldsymbol{v}_{h,\boldsymbol{k}} = S_{h,\boldsymbol{k}} p_{h,\boldsymbol{k}}$. Since the kernels of $S_{h,\boldsymbol{k}}$ and $C_{h,\boldsymbol{k}}$ coincide, the identity $S_{h,\boldsymbol{k}} p_{h,\boldsymbol{k}} = S_{h,\boldsymbol{k}} \hat{C}_{h,\boldsymbol{k}}^{-1} C_{h,\boldsymbol{k}} p_{h,\boldsymbol{k}}$ holds. Together, this defines a projection operator

$$P_{h,\boldsymbol{k}} = \mathrm{id} - S_{h,\boldsymbol{k}} \circ \hat{C}_{h,\boldsymbol{k}}^{-1} \circ B_{h,\boldsymbol{k}} \colon \boldsymbol{V}_{h,\boldsymbol{k}} \longrightarrow \boldsymbol{X}_{h,\boldsymbol{k}} \,,$$

where $\hat{C}_{h,\boldsymbol{k}}^{-1} \colon Q'_{h,\boldsymbol{k}} \longrightarrow \hat{Q}_{h,\boldsymbol{k}}$ gives the solution to a Poisson problem.

In the algorithms below for the eigenvalue computation it will be required that the evaluation of the projection is quite accurate. More precisely, we use an iterative scheme which reduces the initial residual norm by a suitable factor, so that the algebraic error of the approximate projection is considerably smaller than the discretisation error.

2.2.7 Operator properties and finite element convergence

The discretisation $\boldsymbol{X}_{h,\boldsymbol{k}}$ is non-conforming, i. e., $\boldsymbol{X}_{h,\boldsymbol{k}} \not\subset \boldsymbol{X}$. The consistency error of the non-conformity is controlled by the inf-sup stability (2.25), the well-posedness of the inverse follows from the discrete ellipticity (2.12).

The construction of the phase-shifted spaces allows to apply the arguments of Chapter 2.1 (that relate to the case $\boldsymbol{k} = \boldsymbol{0}$) to the actual setting. Especially we have refer to Theorem 2.1.30 for convergence of eigenvalues and eigenfunctions. This method has been developed in [4].

2.2.8 The preconditioned inverse iteration including projections

The inverse iteration is the most simple algorithm for the computation of the smallest eigenvalue and the corresponding eigenmode in the space $\boldsymbol{V}_{h,\boldsymbol{k}}$ of divergence-free functions. Unfortunately, this requires to solve in every step a Maxwell problem in $\boldsymbol{V}_{h,\boldsymbol{k}}$.

In order to get rid of the exact Maxwell solution in every step, we assume that it is sufficient to apply a (linear) preconditioner of the Maxwell problem. Since the Maxwell operator has a large kernel, we consider the shifted operator

$$A_{h,\boldsymbol{k}}^{\delta} = A_{h,\boldsymbol{k}} + \delta M_{h,\boldsymbol{k}} \colon \boldsymbol{V}_{h,\boldsymbol{k}} \longrightarrow \boldsymbol{V}'_{h,\boldsymbol{k}}$$

and the corresponding sesqui-linear form (2.22) for some fixed operator shift $\delta > 0$, and we use in the iteration a preconditioner

$$T_{h,\boldsymbol{k}} \colon \boldsymbol{V}'_{h,\boldsymbol{k}} \longrightarrow \boldsymbol{V}_{h,\boldsymbol{k}}$$

for $A^{\delta}_{h,\boldsymbol{k}}$. We require that the preconditioner is optimal in the sense that $T_{h,\boldsymbol{k}}$ is spectrally equivalent to the inverse of $A^{\delta}_{h,\boldsymbol{k}}$, i.e,

$$C_0\, a^{\delta}_{\boldsymbol{k}}(\boldsymbol{v}_{h,\boldsymbol{k}}, \boldsymbol{v}_{h,\boldsymbol{k}}) \leq a^{\delta}_{\boldsymbol{k}}(T_{h,\boldsymbol{k}} A^{\delta}_{h,\boldsymbol{k}} \boldsymbol{v}_{h,\boldsymbol{k}}, \boldsymbol{v}_{h,\boldsymbol{k}}) \leq C_1\, a^{\delta}_{\boldsymbol{k}}(\boldsymbol{v}_{h,\boldsymbol{k}}, \boldsymbol{v}_{h,\boldsymbol{k}}) \tag{2.26}$$

for all $\boldsymbol{v}_{h,\boldsymbol{k}} \in \boldsymbol{V}_{h,\boldsymbol{k}}$ with constants $C_1 > C_0 > 0$ independent of the mesh size h and the operator shift δ.

It turns out that it is not required to include the divergence constraint into the preconditioner $T_{h,\boldsymbol{k}}$; it is sufficient to include a projection step onto the constrained space $\boldsymbol{X}_{h,\boldsymbol{k}}$ in every iteration. Together, this results in algorithm 1 for the projected inverse iteration.

Algorithm 1 Preconditioned inverse iteration.

(S0) Choose randomly $\boldsymbol{v}_{h,\boldsymbol{k}} \in \boldsymbol{V}_{h,\boldsymbol{k}} \setminus \{0\}$.
(S1) Compute the projection $\boldsymbol{w}_{h,\boldsymbol{k}} = P_{h,\boldsymbol{k}} \boldsymbol{v}_{h,\boldsymbol{k}} \in \boldsymbol{X}_{h,\boldsymbol{k}}$.
(S2) Compute a normalisation

$$\boldsymbol{u}_{h,\boldsymbol{k}} = \frac{1}{\sqrt{m(\boldsymbol{w}_{h,\boldsymbol{k}}, \boldsymbol{w}_{h,\boldsymbol{k}})}}\, \boldsymbol{w}_{h,\boldsymbol{k}}\,.$$

(S3) Compute the eigenvalue approximation

$$\lambda_{h,\boldsymbol{k}} = a_{\boldsymbol{k}}(\boldsymbol{u}_{h,\boldsymbol{k}}, \boldsymbol{u}_{h,\boldsymbol{k}})$$

and the residual

$$\boldsymbol{r}_{h,\boldsymbol{k}} \quad = \quad A_{h,\boldsymbol{k}} \boldsymbol{u}_{h,\boldsymbol{k}} - \lambda_{h,\boldsymbol{k}} M_{h,\boldsymbol{k}} \boldsymbol{u}_{h,\boldsymbol{k}} \in \boldsymbol{X}'_{h,\boldsymbol{k}}\,.$$

(S4) If the residual norm $\|\boldsymbol{r}_{h,\boldsymbol{k}}\|$ is small enough, then STOP.
(S5) Apply the preconditioner: Compute $\boldsymbol{v}_{h,\boldsymbol{k}} := T_{h,\boldsymbol{k}} \boldsymbol{r}_{h,\boldsymbol{k}}$. Go to step (S1).

This method is proposed and analysed in [20], where more details are given. It is observed that the spectral estimate (2.26) transfers to the combined method which includes the projection, i. e. , the condition number of the combined operator $P_{h,\boldsymbol{k}} T_{h,\boldsymbol{k}} A_{h,\boldsymbol{k}}$ (restricted to the constrained space $\boldsymbol{X}_{h,\boldsymbol{k}}$) is bounded independently of the mesh size and the shift parameter.

It turns out that one or two preconditioning steps in (S5) are sufficient. On the other hand, for the evaluation of the projection the approximation by simple preconditioning is not enough (although an exact projection is not required): if the projection is approximated only roughly, the iteration will converge to a vector in the kernel of $A_{h,\boldsymbol{k}}$, i. e., to an eigenvector with eigenvalue 0.

The convergence of this algorithm is linear, provided that the first eigenvalue is isolated. The convergence rate depends on the quotient between first and second eigenvalue. In principle, this can be improved if the operator shift δ is adapted in every iteration step. The optimal choice $\delta = -\lambda_{h,\boldsymbol{k}}$ with the approximated eigenvalue of step (S3) leads to cubic convergence of the eigenvalue iteration, but

it requires to solve nearly indefinite linear problems, so that the iteration with simple preconditioning in (S5) is far more efficient.

2.2.9 The Ritz–Galerkin projection

Since in our application we cannot guarantee that the first eigenvalue is simple, and since we aim for the simultaneous approximation of several eigenvalues in order to identify a band gap, we need a block version of the inverse iteration.

Let $N > 0$ be a small number, e. g., $N = 10$. For a given set $\{\boldsymbol{u}^1_{h,\boldsymbol{k}},\ldots,\boldsymbol{u}^N_{h,\boldsymbol{k}}\} \subset \boldsymbol{X}_{h,\boldsymbol{k}}$ of linear independent functions we can define the Galerkin approximation of the eigenvalue problem (2.23) in the subspace $\boldsymbol{X}^N_{h,\boldsymbol{k}} = \mathrm{Span}\{\boldsymbol{u}^1_{h,\boldsymbol{k}},\ldots,\boldsymbol{u}^N_{h,\boldsymbol{k}}\}$: Set up the Hermitian matrices

$$A_N = \left(a_{\boldsymbol{k}}(\boldsymbol{u}^l_{h,\boldsymbol{k}},\boldsymbol{u}^n_{h,\boldsymbol{k}})\right)_{l,n=1,\ldots,N}, \quad M_N = \left(m(\boldsymbol{u}^l_{h,\boldsymbol{k}},\boldsymbol{u}^n_{h,\boldsymbol{k}})\right)_{l,n=1,\ldots,N} \in \mathbb{C}^{N\times N}$$

and solve a matrix eigenvalue problem: find eigenvectors $z^n \in \mathbb{C}^N \setminus \{0\}$ and eigenvalues $\mu_n \in \mathbb{R}$ with

$$A_N z^n = \mu_n M_N z^n\,, \qquad n = 1,\ldots,N\,, \tag{2.27}$$

where we assume that the eigenvalues are ordered such that $\mu_1 \le \mu_2 \le \cdots \le \mu_N$. We set $(z^1,\ldots,z^N) = \mathcal{Z}(\boldsymbol{u}^1_{h,\boldsymbol{k}},\ldots,\boldsymbol{u}^N_{h,\boldsymbol{k}})$ for this procedure. Then, compute the Ritz–Galerkin projection

$$\boldsymbol{y}^n_{h,\boldsymbol{k}} = \sum_{l=1}^{N} z^n_l \boldsymbol{u}^l_{h,\boldsymbol{k}} \in \boldsymbol{X}_{h,\boldsymbol{k}}\,, \qquad n = 1,\ldots,N\,. \tag{2.28}$$

By construction, we have for $l \neq n$

$$a_{\boldsymbol{k}}(\boldsymbol{y}^l_{h,\boldsymbol{k}},\boldsymbol{y}^n_{h,\boldsymbol{k}}) = 0\,, \qquad m(\boldsymbol{y}^l_{h,\boldsymbol{k}},\boldsymbol{y}^n_{h,\boldsymbol{k}}) = 0\,,$$

and for the Rayleigh quotient

$$\mu_n = \frac{a_{\boldsymbol{k}}(\boldsymbol{y}^n_{h,\boldsymbol{k}},\boldsymbol{y}^n_{h,\boldsymbol{k}})}{m(\boldsymbol{y}^n_{h,\boldsymbol{k}},\boldsymbol{y}^n_{h,\boldsymbol{k}})}\,.$$

The preconditioned inverse iteration can be started simultaneously for the N vectors $\boldsymbol{u}^n_{h,\boldsymbol{k}}$, if in every step a Ritz–Galerkin projection is included. Again, we expect linear convergence of the eigenvalue approximations $\mu_1,\ldots,\mu_n$ to $\lambda^1_{h,\boldsymbol{k}} \le \cdots \le \lambda^n_{h,\boldsymbol{k}}$, provided that for some $1 < n \le N$ a spectral gap $\lambda^{n+1}_{h,\boldsymbol{k}} - \lambda^n_{h,\boldsymbol{k}} > 0$ exists. The convergence factor (in case of exact projections and suitable start vectors) can be estimated by

$$q = 1 - \frac{2}{1 + C_1/C_0}\left(1 - \frac{\lambda^n_{h,\boldsymbol{k}} + \delta}{\lambda^{n+1}_{h,\boldsymbol{k}} + \delta}\right)\,, \tag{2.29}$$

cf. [25, Thm. 9].

2.2.10 The modified LOBPCG method including projections

The LOBPCG method is introduced in [24] in order to improve the convergence of the preconditioned inverse iteration by augmenting the subspace of the Ritz–Galerkin projection. The main idea is inspired by the tree-term recursion of Lanczos method: the Ritz–Galerkin subspace is built of three components, the actual approximations $\boldsymbol{y}^n_{h,\boldsymbol{k}}$, the preconditioned residuals $\boldsymbol{w}^n_{h,\boldsymbol{k}}$, and suitable conjugated directions $\boldsymbol{d}^n_{h,\boldsymbol{k}}$.

Here, we consider the modification introduced by [30] where the preconditioned projected inverse iteration [20] is combined with the LOBPCG method [24], cf. Algorithm 2.

It turns out that this algorithm is far more robust than a simple block version of the preconditioned projected inverse iteration. Nevertheless, a careful choice of stopping criteria is required. In our implementation, we use the following strategies:

(1) In every Ritz–Galerkin step it should be checked with a Gram–Schmidt orthogonalisation, whether the vectors $\boldsymbol{u}^1_{h,\boldsymbol{k}}, \ldots, \boldsymbol{u}^N_{h,\boldsymbol{k}}$ spanning the Ritz–Galerkin subspace are linearly independent: for $n = 2, \ldots, N$ compute

$$\boldsymbol{v}^n_{h,\boldsymbol{k}} = \boldsymbol{u}^n_{h,\boldsymbol{k}} - \sum_{l=1}^{n-1} m(\boldsymbol{u}^l_{h,\boldsymbol{k}}, \boldsymbol{u}^n_{h,\boldsymbol{k}})\, \boldsymbol{u}^l_{h,\boldsymbol{k}}$$

so that $\boldsymbol{v}^n_{h,\boldsymbol{k}}$ is orthogonal to $\boldsymbol{u}^1_{h,\boldsymbol{k}}, \ldots, \boldsymbol{u}^{n-1}_{h,\boldsymbol{k}}$. If $\|\boldsymbol{v}^n_{h,\boldsymbol{k}}\| = \sqrt{m(\boldsymbol{v}^n_{h,\boldsymbol{k}}, \boldsymbol{v}^n_{h,\boldsymbol{k}})} \geq \epsilon_1$, set $\boldsymbol{u}^n_{h,\boldsymbol{k}} = \boldsymbol{v}^n_{h,\boldsymbol{k}} / \|\boldsymbol{v}^n_{h,\boldsymbol{k}}\|$. Otherwise, the vector $\boldsymbol{v}^n_{h,\boldsymbol{k}}$ is nearly linearly depending from $\boldsymbol{u}^1_{h,\boldsymbol{k}}, \ldots, \boldsymbol{u}^{n-1}_{h,\boldsymbol{k}}$. Then, $\boldsymbol{u}^n_{h,\boldsymbol{k}}$ is replaced by a new random vector and the orthogonalisation procedure is repeated.
Here, $\epsilon_1 = 10^{-8}$ is appropriate, if the stopping criterion for the residual is not too small.

(2) The projections $\boldsymbol{w}^n_{h,\boldsymbol{k}} = P_{h,\boldsymbol{k}} \boldsymbol{v}^n_{h,\boldsymbol{k}}$ in (S0) and (S2) are computed only approximately: we compute $q_{h,\boldsymbol{k}} \in Q_{h,\boldsymbol{k}}$ such that $\|C_{h,\boldsymbol{k}} q_{h,\boldsymbol{k}} - B_{h,\boldsymbol{k}} \boldsymbol{v}^n_{h,\boldsymbol{k}}\| \leq \epsilon_2 + \theta_2 \|B_{h,\boldsymbol{k}} \boldsymbol{v}^n_{h,\boldsymbol{k}}\|$ and set $\boldsymbol{w}^n_{h,\boldsymbol{k}} = \boldsymbol{v}^n_{h,\boldsymbol{k}} - S_{h,\boldsymbol{k}} q_{h,\boldsymbol{k}} \in \boldsymbol{V}_{h,\boldsymbol{k}}$, i. e., in general $\boldsymbol{w}^n_{h,\boldsymbol{k}} \notin \boldsymbol{X}_{h,\boldsymbol{k}}$.
Here, $\epsilon_2 = 10^{-8}$ and a residual reduction $\theta_2 = 10^{-7}$ is appropriate. For simplicity, one can use a simple Euclidean vector norm since the strong residual reduction already ensures that the relative error is small enough.
Note that the eigenvalue accuracy which can be obtained with the projected LOBPCG method is strictly limited by the accuracy of the projection.

(3) On the other hand, the algorithm does not require an accurate solution of the preconditioning step in (S2). In our implementation it is realised as follows: we apply a few iterations of a Krylov method (preconditioned with $T_{h,\boldsymbol{k}}$) such that $\|A^\delta_{h,\boldsymbol{k}} \boldsymbol{v}^n_{h,\boldsymbol{k}} - \boldsymbol{r}^n_{h,\boldsymbol{k}}\| \leq \epsilon_3 + \theta_3 \|\boldsymbol{r}^n_{h,\boldsymbol{k}}\|$. Moreover, we observe that the algorithm is not sensitive with respect to the operator shift $\delta > 0$ (in

Algorithm 2 The modified LOPCG method

(S0) Choose random vectors $\boldsymbol{v}^1_{h,\boldsymbol{k}}, \ldots, \boldsymbol{v}^N_{h,\boldsymbol{k}} \in \boldsymbol{V}_{h,\boldsymbol{k}}$.
For $n = 1, \ldots, N$, compute the projections and normalisations

$$\boldsymbol{w}^n_{h,\boldsymbol{k}} = P_{h,\boldsymbol{k}} \boldsymbol{v}^n_{h,\boldsymbol{k}} \in \boldsymbol{X}_{h,\boldsymbol{k}}\,, \qquad \boldsymbol{u}_{h,\boldsymbol{k}} = \frac{1}{\sqrt{m(\boldsymbol{w}_{h,\boldsymbol{k}}, \boldsymbol{w}_{h,\boldsymbol{k}})}}\, \boldsymbol{w}_{h,\boldsymbol{k}}\,.$$

Then, compute the Ritz–Galerkin eigenvalues $\lambda^1, \ldots, \lambda^N$ and eigenvectors

$$(z^1, \ldots, z^N) = \mathcal{Z}(\boldsymbol{u}^1_{h,\boldsymbol{k}}, \ldots, \boldsymbol{u}^N_{h,\boldsymbol{k}})$$

and the Ritz–Galerkin projection

$$\boldsymbol{y}^n_{h,\boldsymbol{k}} = \sum_{m=1}^{N} z^n_m \boldsymbol{u}^m_{h,\boldsymbol{k}} \in \boldsymbol{X}_{h,\boldsymbol{k}}\,, \qquad n = 1, \ldots, N\,.$$

(S1) For $n = 1, \ldots, N$, compute the residuals

$$\boldsymbol{r}^n_{h,\boldsymbol{k}} = A_{h,\boldsymbol{k}} \boldsymbol{y}^n_{h,\boldsymbol{k}} - \lambda^n M_{h,\boldsymbol{k}} \boldsymbol{y}^n_{h,\boldsymbol{k}} \in \boldsymbol{V}'_{h,\boldsymbol{k}}\,,$$

and check for convergence.

(S2) For $n = 1, \ldots, N$, apply the preconditioner $\boldsymbol{v}^n_{h,\boldsymbol{k}} = T_{h,\boldsymbol{k}} \boldsymbol{r}^n_{h,\boldsymbol{k}} \in \boldsymbol{V}_{h,\boldsymbol{k}}$ and compute the projection $\boldsymbol{w}^n_{h,\boldsymbol{k}} := P_{h,\boldsymbol{k}} \boldsymbol{v}^n_{h,\boldsymbol{k}} \in \boldsymbol{X}_{h,\boldsymbol{k}}$.

(S3) Perform this step in the first iteration; otherwise go to (S4).
Compute the Ritz–Galerkin eigenvectors

$$(z^1, \ldots, z^{2N}) = \mathcal{Z}(\boldsymbol{w}^1_{h,\boldsymbol{k}}, \ldots, \boldsymbol{w}^N_{h,\boldsymbol{k}}, \boldsymbol{y}^1_{h,\boldsymbol{k}}, \ldots, \boldsymbol{y}^N_{h,\boldsymbol{k}})\,.$$

For $n = 1, \ldots, N$, set

$$\begin{aligned} \boldsymbol{d}^n_{h,\boldsymbol{k}} &= \sum_{l=1}^{N} z^n_l \boldsymbol{w}^l_{h,\boldsymbol{k}} \in \boldsymbol{X}_{h,\boldsymbol{k}}\,, \\ \tilde{\boldsymbol{y}}^n_{h,\boldsymbol{k}} &= \boldsymbol{d}^n_{h,\boldsymbol{k}} + \sum_{l=1}^{N} z^n_{N+l} \boldsymbol{y}^l_{h,\boldsymbol{k}} \in \boldsymbol{X}_{h,\boldsymbol{k}}\,. \end{aligned}$$

Then, set $\boldsymbol{y}^n_{h,\boldsymbol{k}} = \tilde{\boldsymbol{y}}^n_{h,\boldsymbol{k}}$ for $n = 1, \ldots, N$. Go to (S1).

(S4) Compute the Ritz–Galerkin eigenvectors

$$(z^1, \ldots, z^{3N}) = \mathcal{Z}(\boldsymbol{w}^1_{h,\boldsymbol{k}}, \ldots, \boldsymbol{w}^N_{h,\boldsymbol{k}}, \boldsymbol{y}^1_{h,\boldsymbol{k}}, \ldots, \boldsymbol{y}^N_{h,\boldsymbol{k}}, \boldsymbol{d}^1_{h,\boldsymbol{k}}, \ldots, \boldsymbol{d}^N_{h,\boldsymbol{k}})\,.$$

For $n = 1, \ldots, N$, set

$$\begin{aligned} \tilde{\boldsymbol{d}}^n_{h,\boldsymbol{k}} &= \sum_{l=1}^{N} z^n_l \boldsymbol{w}^l_{h,\boldsymbol{k}} + z^n_{2N+l} \boldsymbol{d}^l_{h,\boldsymbol{k}}\,, \\ \tilde{\boldsymbol{y}}^n_{h,\boldsymbol{k}} &= \tilde{\boldsymbol{d}}^n_{h,\boldsymbol{k}} + \sum_{l=1}^{N} z^n_{N+l} \boldsymbol{y}^l_{h,\boldsymbol{k}}\,. \end{aligned}$$

Then, set $\boldsymbol{y}^n_{h,\boldsymbol{k}} = \tilde{\boldsymbol{y}}^n_{h,\boldsymbol{k}}$ and $\boldsymbol{d}^n_{h,\boldsymbol{k}} = \tilde{\boldsymbol{d}}^n_{h,\boldsymbol{k}}$ for $n = 1, \ldots, N$. Go to (S1).

particular, $A^{\delta}_{h,\boldsymbol{k}}$ and $A_{h,\boldsymbol{k}}$ have the same eigenvectors). From (2.29) we can estimate that a residual reduction $\theta_3 = 0.1$ and an operator shift $\delta = 0.1\lambda^1_{\boldsymbol{k},h}$ is a suitable choice (indeed, a further reduction to a smaller $\delta > 0$ or a smaller θ_3 does not reduce the required number of LOBPCG steps).

(4) After a few LOBPCG iteration steps the smallest eigenvalues are already very accurate (if N is large enough). Depending on the accuracy of the projection it may be not possible to improve the corresponding eigenmode. So in step (S1) we determine $0 \le n_{\mathrm{conv}} \le N$ such that $\|\boldsymbol{r}^n_{h,\boldsymbol{k}}\| \le \epsilon_4$ for $n = 1, \dots, n_{\mathrm{conv}}$. Then, we proceed the method with the vectors

$$\boldsymbol{w}^{n_{\mathrm{conv}}+1}_{h,\boldsymbol{k}}, \dots, \boldsymbol{w}^{N}_{h,\boldsymbol{k}}, \boldsymbol{y}^{n_{\mathrm{conv}}+1}_{h,\boldsymbol{k}}, \dots, \boldsymbol{y}^{N}_{h,\boldsymbol{k}}, \boldsymbol{d}^{n_{\mathrm{conv}}+1}_{h,\boldsymbol{k}}, \dots, \boldsymbol{d}^{N}_{h,\boldsymbol{k}}$$

in step (S4).
The overall procedure is more efficient if N is larger than the desired number of eigenvalues. Thus, one should stop the LOBPCG iteration if $n_{\mathrm{conv}} \ge N/2$. Here, $\epsilon_4 \approx \sqrt{\epsilon_2}$ is appropriate. Then, we can expect a relative accuracy of $\epsilon_4^2 \approx \epsilon_2$ for the eigenvalues. Since in this stopping criterion the residual norm is used for estimating the error, a mesh-independent evaluation is required. This is obtained, e. g., by the application of the preconditioner: set

$$\|\boldsymbol{r}^n_{h,\boldsymbol{k}}\| = \sqrt{\langle \boldsymbol{r}^n_{h,\boldsymbol{k}}, \boldsymbol{w}^n_{h,\boldsymbol{k}} \rangle} = \sqrt{\langle \boldsymbol{r}^n_{h,\boldsymbol{k}}, T_{k,\boldsymbol{k}} \boldsymbol{r}^n_{h,\boldsymbol{k}} \rangle}\,.$$

A simple alternative (which avoids to apply the preconditioner) is to use one sweep of a Gauss–Seidel relaxation $R_{j,\boldsymbol{k}} \colon \boldsymbol{V}'_{j,\boldsymbol{k}} \longrightarrow \boldsymbol{V}_{j,\boldsymbol{k}}$ for $A_{j,\boldsymbol{k}}$, i. e., to use $\|\boldsymbol{r}^n_{h,\boldsymbol{k}}\| = \sqrt{\langle \boldsymbol{r}^n_{h,\boldsymbol{k}}, R_{k,\boldsymbol{k}} \boldsymbol{r}^n_{h,\boldsymbol{k}} \rangle}$.

More details on different variants of the LOBPCG method and the suitable choice of parameters are discussed in [9].

2.2.11 A multigrid preconditioner for the Maxwell operator

A suitable multigrid preconditioner $T_{j,\boldsymbol{k}} \colon \boldsymbol{V}'_{j,\boldsymbol{k}} \longrightarrow \boldsymbol{V}_{j,\boldsymbol{k}}$ satisfying (2.26) with $C_1 > C_0 > 0$ independent of the mesh size and robust for $0 < \delta \le \delta_0$ is introduced by Hiptmair [18]. Therefore, let $\boldsymbol{V}_{0,\boldsymbol{k}} \subset \boldsymbol{V}_{1,\boldsymbol{k}} \subset \cdots \subset \boldsymbol{V}_{J,\boldsymbol{k}} \subset \boldsymbol{V}$ be a nested sequence of curl-conforming finite element spaces with phase-shifted basis and with mesh size $h_j = 2^{-j} h_0$ on level $j = 0, \dots, J$, and let $Q_{0,\boldsymbol{k}} \subset Q_{1,\boldsymbol{k}} \subset \cdots \subset Q_{J,\boldsymbol{k}} \subset Q$ be the corresponding H^1-conforming spaces with phase-shifted basis.

The main observation is that a stable splitting corresponding to the decomposition

$$\boldsymbol{V}_{J,\boldsymbol{k}} = \boldsymbol{V}_{0,\boldsymbol{k}} + \sum_{j=1}^{J} \boldsymbol{V}_{j,\boldsymbol{k}} + \sum_{j=1}^{J} \boldsymbol{\nabla}_{\boldsymbol{k}} Q_{j,\boldsymbol{k}}$$

with respect to the energy norm of $A^{\delta}_{J,\boldsymbol{k}}$ exists. As a consequence we obtain multigrid convergence for a hybrid smoother which alternatively operates on $\boldsymbol{V}_{j,\boldsymbol{k}}$ and

$\boldsymbol{\nabla}_{\boldsymbol{k}} Q_{j,\boldsymbol{k}}$. The multigrid preconditioner is defined recursively: for $j = 0$, define $T_{0,\boldsymbol{k}} = \left(A^{\delta}_{0,\boldsymbol{k}}\right)^{-1}$. For $j > 0$, the definition of $T_{j,\boldsymbol{k}}$ requires:

1) a prolongation operator $I_{j,\boldsymbol{k}} \colon \boldsymbol{V}_{j-1,\boldsymbol{k}} \longrightarrow \boldsymbol{V}_{j,\boldsymbol{k}}$;
2) the adjoint operator (restriction operator) $I'_{j,\boldsymbol{k}} \colon \boldsymbol{V}'_{j,\boldsymbol{k}} \longrightarrow \boldsymbol{V}'_{j-1,\boldsymbol{k}}$;
3) a smoother $R_{j,\boldsymbol{k}} \colon \boldsymbol{V}'_{j,\boldsymbol{k}} \longrightarrow \boldsymbol{V}_{j,\boldsymbol{k}}$ for $A_{j,\boldsymbol{k}}$;
4) a smoother $D_{j,\boldsymbol{k}} \colon Q'_{j,\boldsymbol{k}} \longrightarrow Q_{j,\boldsymbol{k}}$ for $C_{j,\boldsymbol{k}}$;
5) a transfer operator $S_{j,\boldsymbol{k}} \colon Q_{j,\boldsymbol{k}} \longrightarrow \boldsymbol{V}_{j,\boldsymbol{k}}$;
6) the adjoint transfer operator $S'_{j,\boldsymbol{k}} \colon \boldsymbol{V}'_{j,\boldsymbol{k}} \longrightarrow Q'_{j,\boldsymbol{k}}$.

Now, define $T_{j,\boldsymbol{k}}$ by

$$\begin{aligned}&\mathrm{id} - A^{\delta}_{j,\boldsymbol{k}} T_{j,\boldsymbol{k}} \\ &\quad = \left(\mathrm{id} - A^{\delta}_{j,\boldsymbol{k}} I_{j,\boldsymbol{k}} T_{j-1,\boldsymbol{k}} I'_{j,\boldsymbol{k}}\right)\left(\mathrm{id} - \delta^{-1} A^{\delta}_{j,\boldsymbol{k}} S_{j,\boldsymbol{k}} D_{j,\boldsymbol{k}} S'_{j,\boldsymbol{k}}\right)^{\nu}\left(\mathrm{id} - A^{\delta}_{j,\boldsymbol{k}} R_{j,\boldsymbol{k}}\right)^{\mu}.\end{aligned}$$

For given residual $r_{J,\boldsymbol{k}}$, the result $v_{J,\boldsymbol{k}} = T_{J,\boldsymbol{k}} r_{J,\boldsymbol{k}}$ is computed by Algorithm 3.

Algorithm 3 Multigrid preconditioner $v_{J,\boldsymbol{k}} = T_{J,\boldsymbol{k}} r_{J,\boldsymbol{k}}$ with hybrid smoother.

(S0) Set $j = J$.
(S1) Set $v_{j,\boldsymbol{k}} = 0$. For $\kappa = 1, \ldots, \mu$ compute

$$\begin{aligned} w_{j,\boldsymbol{k}} &= R_{j,\boldsymbol{k}} r_{j,\boldsymbol{k}}\,, \\ v_{j,\boldsymbol{k}} &:= v_{j,\boldsymbol{k}} + w_{j,\boldsymbol{k}}\,, \\ r_{j,\boldsymbol{k}} &:= r_{j,\boldsymbol{k}} - A^{\delta}_{j,\boldsymbol{k}} w_{j,\boldsymbol{k}}\,. \end{aligned}$$

(S2) For $\kappa = 1, \ldots, \nu$ compute

$$\begin{aligned} w_{j,\boldsymbol{k}} &= \delta^{-1} A^{\delta}_{j,\boldsymbol{k}} S_{j,\boldsymbol{k}} D_{j,\boldsymbol{k}} S'_{j,\boldsymbol{k}} r_{j,\boldsymbol{k}}\,, \\ v_{j,\boldsymbol{k}} &:= v_{j,\boldsymbol{k}} + w_{j,\boldsymbol{k}}\,, \\ r_{j,\boldsymbol{k}} &:= r_{j,\boldsymbol{k}} - A^{\delta}_{j,\boldsymbol{k}} w_{j,\boldsymbol{k}}\,. \end{aligned}$$

(S3) If $j > 0$, set $r_{j-1,\boldsymbol{k}} = I'_{j,\boldsymbol{k}} r_{j,\boldsymbol{k}}$, $j := j - 1$, and go to (S1).
(S4) If $j = 0$, set $v_{0,\boldsymbol{k}} := T_{0,\boldsymbol{k}} r_{0,\boldsymbol{k}}$.
(S5) For $j = 1, \ldots, J$ set

$$v_{j,\boldsymbol{k}} := v_{j,\boldsymbol{k}} + I_{j,\boldsymbol{k}} v_{j-1,\boldsymbol{k}}\,.$$

Return the result $v_{J,\boldsymbol{k}}$.

The prolongation is defined by the simple embedding $\boldsymbol{V}_{j-1,\boldsymbol{k}} \subset \boldsymbol{V}_{j,\boldsymbol{k}}$, i. e.,

$$I_{j,\boldsymbol{k}} \boldsymbol{v}_{j-1,\boldsymbol{k}} = \sum_{e \in \mathcal{E}_j} \langle \boldsymbol{\psi}'_{e,\boldsymbol{k}}, \boldsymbol{v}_{j-1,\boldsymbol{k}} \rangle \boldsymbol{\psi}_{e,\boldsymbol{k}}\,,$$

and it is represented by the matrix $\underline{I}_{j,\boldsymbol{k}} = \big(\underline{I}_{e_1,e_2}\big)_{(e_1,e_2)\in\mathcal{E}_j\times\mathcal{E}_{j-1}}$

$$I_{j,\boldsymbol{k}} = \sum_{(e_1,e_2)\in\mathcal{E}_j\times\mathcal{E}_{j-1}} \underline{I}_{e_1,e_2}\boldsymbol{\psi}'_{e_2,\boldsymbol{k}}\otimes\boldsymbol{\psi}_{e_1,\boldsymbol{k}}\,, \qquad \underline{I}_{e_1,e_2} = \langle\boldsymbol{\psi}'_{e_1,\boldsymbol{k}},\boldsymbol{\psi}_{e_2,\boldsymbol{k}}\rangle\,.$$

The restriction is represented by the transposed matrix $\underline{I}^T_{j,\boldsymbol{k}}$, i. e.,

$$I'_{j,\boldsymbol{k}} = \sum_{(e_2,e_1)\in\mathcal{E}_{j-1}\times\mathcal{E}_j} \underline{I}_{e_1,e_2}\boldsymbol{\psi}_{e_1,\boldsymbol{k}}\otimes\boldsymbol{\psi}'_{e_2,\boldsymbol{k}}\,.$$

Note that this implies that the transfer operators depend on the phase-shift, but again (as it is observed in Chapter 2.2.4) by a simple scaling the operators can be constructed from the standard operators for $\boldsymbol{k}=\boldsymbol{0}$.

The smoothing operators are constructed algebraically from the matrix representations of $A_{j,\boldsymbol{k}}$ and $C_{j,\boldsymbol{k}}$. E. g., the Gauss–Seidel relaxation is defined by

$$R_{j,\boldsymbol{k}} = \sum_{e_1,e_2\in\mathcal{E}_j} \underline{R}_{e_1,e_2}\boldsymbol{\psi}_{e_2,\boldsymbol{k}}\otimes\boldsymbol{\psi}_{e_1,\boldsymbol{k}}\,, \qquad \underline{R}_{j,\boldsymbol{k}} = \Big(\operatorname{diag}\underline{A}_{j,\boldsymbol{k}} + \operatorname{lower}\underline{A}_{j,\boldsymbol{k}}\Big)^{-1},$$

$$D_{h,\boldsymbol{k}} = \sum_{v_1,v_2\in\mathcal{V}_h} \underline{D}_{v_1,v_2}\phi_{v_2,\boldsymbol{k}}\otimes\phi_{v_1,\boldsymbol{k}}\,, \qquad \underline{D}_{j,\boldsymbol{k}} = \Big(\operatorname{diag}\underline{C}_{j,\boldsymbol{k}} + \operatorname{lower}\underline{D}_{j,\boldsymbol{k}}\Big)^{-1}.$$

Note that Gauss–Seidel smoothing depends on the numbering of the indices.

For the parallel smoothers $R_{j,\boldsymbol{k}}$ and $D_{j,\boldsymbol{k}}$ suitable damping is required; in addition, we use multiple smoothing $\nu,\mu>1$, and we use a symmetric variant of the presented algorithm.

In the same way, we construct the Laplace preconditioner $U_{j,\boldsymbol{k}}\colon Q'_{j,\boldsymbol{k}}\longrightarrow Q_{j,\boldsymbol{k}}$ within the projection step. Again we set $U_{0,\boldsymbol{k}} = C^{-1}_{0,\boldsymbol{k}}$, and recursively $U_{j,\boldsymbol{k}}$ is defined for $j>0$ by

$$\mathrm{id} - C_{j,\boldsymbol{k}}U_{j,\boldsymbol{k}} \;=\; \big(\mathrm{id} - C_{j,\boldsymbol{k}}J_{j,\boldsymbol{k}}U_{j-1,\boldsymbol{k}}J'_{j,\boldsymbol{k}}\big)\big(\mathrm{id} - C_{j,\boldsymbol{k}}D_{j-1,\boldsymbol{k}}\big)^{\nu},$$

where $J_{j,\boldsymbol{k}}\colon Q_{j-1,\boldsymbol{k}}\longrightarrow Q_{j,\boldsymbol{k}}$ and $J'_{j,\boldsymbol{k}}\colon Q'_{j,\boldsymbol{k}}\longrightarrow Q'_{j-1,\boldsymbol{k}}$ are the prolongation and restriction operators, respectively (again obtained from the standard transfer operators by a scaling with respect to the phase-shift).

2.2.12 Numerical results for a band gap computation

Finally, we summarise results from [9] for the eigenvalue computation of a specific configuration. The computation is realised in the parallel finite element code M++ [28] which supports fully parallel multigrid methods [29].

We consider a material distribution proposed in [16], where we use a material with permittivity $\varepsilon_{\mathrm{r}} = 13$ (which is in a realistic range for, e. g., silicon), and for the empty space we have $\varepsilon_{\mathrm{r}} = 1$. The distribution is a layered structure, cf. Fig. 2.1. The structure is highly symmetric in xy plane, but is not symmetric

in z direction. The configuration consists of silicon blocks, the block thickness in the periodic structure is 0.25. We start in level 0 with one hexahedron, then we use regular refinement, see Tab. 2.1. Thus, level 3 is the minimal level where the material distribution is represented exactly, i. e., the distributions is aligned with the cells.

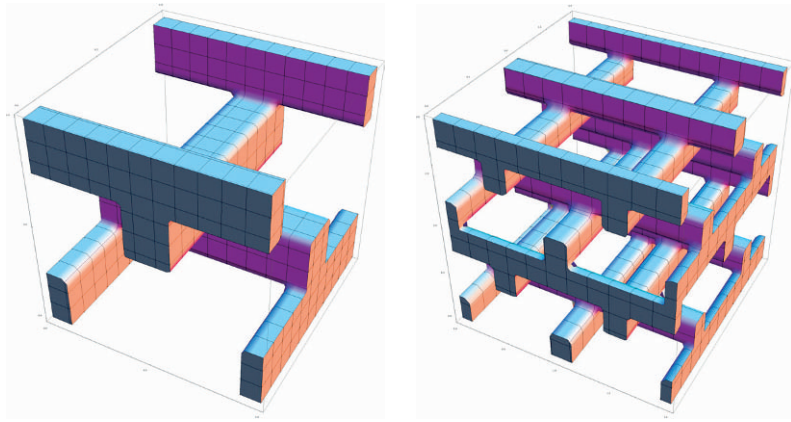

Figure 2.1: A layered structure in the periodicity cell $[0,1]^3$ (left) and (for illustration) in $[0,2]^3$ showing 8 periodicity cells (right).

level j	number of cells	d.o.f. in $\boldsymbol{X}_h$	d.o.f. in Q_h
2	64		
3	512	1 944	729
4	4 096	13 872	4 913
5	32 768	104 544	35 937
6	262 144	811 200	274 625
7	2 097 152	6 390 144	2 146 689
8	16 777 216	50 725 632	16 974 593

Table 2.1: Refinement levels, number of cells and degrees of freedom for the test configuration.

We test the convergence properties of the LOBPCG method for a fixed parameter $\boldsymbol{k} = (3, 1, -2)$, where we use $\epsilon_4 = 10^{-4}$ as stopping criterion. The results in Tab. 2.2 indicates that the convergence is almost independent of the mesh size, and that the number of iterations only slowly increases with the number of computed eigenvalues.

All results are obtained on a parallel Linux cluster. Since the multigrid solver is of optimal complexity, we expect an optimal scaling behaviour of the parallel

N #	level 3	level 4	level 5	level 6
1	6	6	6	7
2	6	7	7	7
3	7	7	7	8
4	7	8	8	8
5	9	10	10	11
6	9	10	11	11
7	11	12	12	12
8	11	12	12	12
9	12	13	13	13
10	12	13	14	14

Table 2.2: Number of iterations of the projected LOBPCG method for the convergence of the first N eigenvalues and eigenvectors depending on the refinement level.

algorithm, provided the coarse problem is fine enough. For a fixed-size numerical performance test (cf. Tab. 2.3) we observe good scalability only up to 256 processor kernels. Optimal scalability is obtain for fixed load per processor kernel up to 50 million unknowns, cf. Tab. 2.4.

processor kernels	multigrid aver. conv. rate	computing time	scaling factor
64	0.28	37:47 min.	2.12
128	0.28	17:45 min.	1.80
256	0.27	9:54 min.	1.19
512	0.29	8:20 min.	

Table 2.3: Fixed-size parallel scalability and Maxwell multigrid convergence on refinement level 7.

Next, we study the eigenvalue convergence. Again, we fix the parameter $\boldsymbol{k} = (3, 1, -2)$, and we set $\epsilon_4 = 10^{-4}$ for the defect precision. Then, at least for isolated eigenvalues we may expect algebraic eigenvector convergence $O(\epsilon_4)$ and eigenvalue convergence $O(\epsilon_4^2)$, so that we can assume that the discretisation error is much larger than the algebraic truncation error. The eigenvalue results are presented in Tab. 2.5, and from their asymptotic behaviour we estimate the convergence rate in Tab. 2.6. For smooth eigenfunctions $O(h^2)$ convergence can be expected, but due to the poor regularity resulting from the discontinuous permittivity the observed convergence rate with respect to the mesh size are smaller.

refinement level	d.o.f.	computing time	scaling factor
5	104,544	1:05 min.	
			1.78
6	811,200	1:56 min.	
			5.12
7	6,390,144	9:54 min.	
			8.09
8	50,725,632	80:21 min.	

Table 2.4: Fixed-load parallel performance on 256 processor kernels.

n	level 3	level 4	level 5	level 6	level 7	level 8
1	3.86613	3.81920	3.80119	3.79449	3.79202	3.79111
2	4.13949	4.09004	4.07099	4.06392	4.06132	4.06036
3	5.01881	4.87990	4.82904	4.81021	4.80322	4.80063
4	5.38737	5.24131	5.18723	5.16714	5.15967	5.15690
5	10.19397	9.68279	9.54135	9.50006	9.48747	9.48348
6	10.46622	9.95338	9.80933	9.76693	9.75392	9.74977
7	12.22023	11.26907	11.02740	10.95948	10.93931	10.93307
8	12.35505	11.40819	11.16670	11.09883	11.07870	11.07247
9	13.78493	12.78181	12.51608	12.43920	12.41575	12.40829
10	13.95290	12.93797	12.66950	12.59189	12.56823	12.56071

Table 2.5: Eigenvalue results $\lambda_{j,\boldsymbol{k}}^n$, $n = 1, \ldots, N$, for different refinement levels j.

Finally, we collect the results for different $\boldsymbol{k}$ following a path in the Brillouin zone. The result illustrates the band structure, cf. Fig. 2.3. Although this path does not cover the full Brillouin zone, one expects extrema in the photonic bands on the boundary of the Brillouin zone or at points with high symmetry, so that we can assume that this figure provides the correct band gap information of the given material distribution. Guaranteed band gap computations can be obtained by a finite number of further eigenvalue computations (including upper and lower eigenvalue bounds) and a suitable perturbation argument (cf. [21]).

Note that the eigenfunctions within the Floquet theory are abstract constructions and not physical objects; nevertheless, some illustrations are presented in Fig. 2.4 and 2.5.

n	$\Delta^n(3,4)$		$\Delta^n(4,5)$		$\Delta^n(5,6)$		$\Delta^n(6,7)$		$\Delta^n(7,8)$
1	0.04693	1.38	0.01801	1.43	0.00669	1.44	0.00247	1.44	0.00091
2	0.04945	1.38	0.01905	1.43	0.00707	1.44	0.00260	1.44	0.00096
3	0.13891	1.45	0.05087	1.43	0.01883	1.43	0.00698	1.43	0.00259
4	0.14607	1.43	0.05407	1.43	0.02009	1.43	0.00747	1.43	0.00277
5	0.51118	1.85	0.14144	1.78	0.04130	1.71	0.01259	1.66	0.00399
6	0.51284	1.83	0.14405	1.76	0.04240	1.70	0.01301	1.65	0.00415
7	0.95116	1.98	0.24167	1.83	0.06792	1.75	0.02017	1.69	0.00625
8	0.94685	1.97	0.24149	1.83	0.06787	1.75	0.02013	1.69	0.00623
9	1.00313	1.92	0.26573	1.79	0.07687	1.71	0.02346	1.65	0.00746
10	1.01493	1.92	0.26847	1.79	0.07761	1.71	0.02366	1.65	0.00752

Table 2.6: The eigenvalue convergence rate is estimated by $\Delta^n(j-1,j) = |\lambda^n_{j-1,\boldsymbol{k}} - \lambda^n_{j,\boldsymbol{k}}|$ and the factor $\log_2\big(\Delta^n(j-1,j)/\Delta^n(j,j+1)\big)$.

Bibliography

[1] D. Boffi. Fortin elements and discrete compactness for edge elements. *Numer. Math.*, 87:229–246, 2000.

[2] D. Boffi. Finite element approximations of eigenvalue problems. *Acta Numerica*, 19:1–120, 2010.

[3] D. Boffi, F. Brezzi, and L. Gastaldi. On the convergence of eigenvalues for mixed formulations. *Ann. Scuola Norm. Sup. Pisa Cl. Sci.* (4), 25:131–154, 1997.

[4] D. Boffi, M. Conforti, and L. Gastaldi. Modified edge finite elements for photonic crystals. *Numerische Mathematik*, 105(2):249–266, 2006.

[5] D. Boffi, L. Demkowicz, and M. Costabel. Discrete compactness for p and hp 2d edge finite elements. *Math. Models Methods Appl. Sci.*, 13:1673–1687, 2003.

[6] D. Boffi and L. Gastaldi. Interpolation estimates for edge finite elements and application to band gap computation. *Appl. Numer. Math.*, 56:1283–1292, 2006.

[7] A. Bonito and J.-L. Guermond. Approximation of the eigenvalue problem for the time harmonic Maxwell system by continuous Lagrange finite elements, 2009. Report IAMCS 2009–121, Texas A&M.

[8] S. C. Brenner and L. R. Scott. *The mathematical theory of finite element methods*, volume 15 of *Texts in Applied Mathematics*. Springer, New York, 1994.

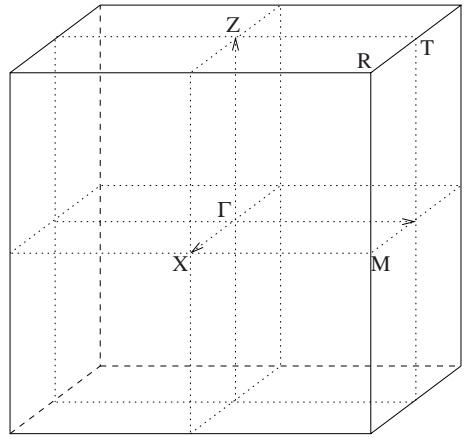

Figure 2.2: The Brillouin zone and the points of high symmetry.

[9] A. Bulovyatov. *Parallel multigrid methods for the band structure computation of 3D photonic crystals with higher order finite elements*. Ph.D. thesis, Karlsruhe Institute of Technology, 2010.

[10] S. Caorsi, P. Fernandes, and M. Raffetto. On the convergence of Galerkin finite element approximations of electromagnetic eigenproblems. *SIAM J. Numer. Anal.*, 38:580–607, 2000.

[11] P. Ciarlet Jr. and G. Hechme. Computing electromagnetic eigenmodes with continuous Galerkin approximations. *Comput. Methods Appl. Mech. Engrg.*, 198:358–365, 2008.

[12] M. Costabel and M. Dauge. Maxwell and Lamé eigenvalues on polyhedra. *Math. Methods Appl. Sci.*, 22:243–258, 1999.

[13] M. Costabel and M. Dauge. Weighted regularization of Maxwell equations in polyhedral domains. A rehabilitation of nodal finite elements. *Numer. Math.*, 93:239–277, 2002.

[14] M. Costabel, M. Dauge, and S. Nicaise. Singularities of Maxwell interface problems. *Math. Model. Numer. Anal.*, 33:627–649, 1999.

[15] L. Demkowicz, P. Monk, C. Schwab, and L. Vardapetyan. Maxwell eigenvalues and discrete compactness in two dimensions. *Comput. Math. Appl.*, 40:589–605, 2000.

[16] D. C. Dobson, Jayadeep Gopalakrishnan, and J. E. Pasciak. An efficient method for band structure calculations in 3D photonic crystals. *Journal of Computational Physics*, 161(2):668–679, 2000.

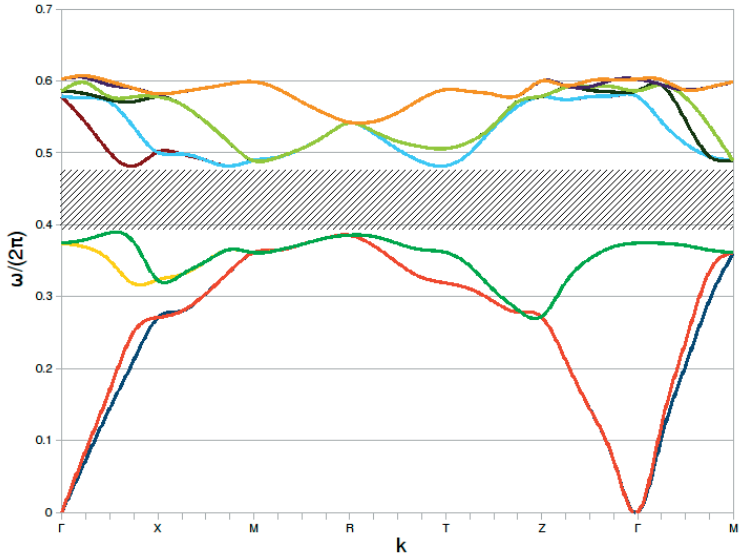

Figure 2.3: Band structure illustration along a curve in the Brillouin zone along the points Γ, X, M, R, T, and Z (cf. Fig. 2.2). A band gap is observed between the bands 4 and 5.

[17] A. Ern and J.-L. Guermond. *Theory and practice of finite elements*, volume 159 of *Applied Mathematical Sciences*. Springer, New York, 2004.

[18] R. Hiptmair. Multigrid method for Maxwell's equations. *SIAM Journal on Numerical Analysis*, 36(1):204–225, 1998.

[19] R. Hiptmair. Finite elements in computational electromagnetism. *Acta Numerica*, 11:237–339, 2002.

[20] R. Hiptmair and K. Neymeyr. Multilevel method for mixed eigenproblems. *SIAM Journal on Scientific Computing*, 23(6):2141–2164, 2002.

[21] V. Hoang, M. Plum, and C. Wieners. A computer-assisted proof for photonic band gaps. *Zeitschrift für Angewandte Mathematik und Physik*, 60:1–18, 2009.

[22] F. Kikuchi. On a discrete compactness property for the Nédélec finite elements. *J. Fac. Sci. Univ. of Tokio Sec. IA*, 36:479–490, 1989.

[23] F. Kikuchi. Mixed Formulations for Finite Element Analysis of Magnetostatic and Electrostatic Problems. *Japan J. Appl. Math.*, 6:209–221, 1989.

[24] A. V. Knyazev. Toward the optimal preconditioned eigensolver: locally optimal block preconditioned conjugate gradient method. *SIAM Journal on Scientific Computing*, 23(2):517–541, 2001.

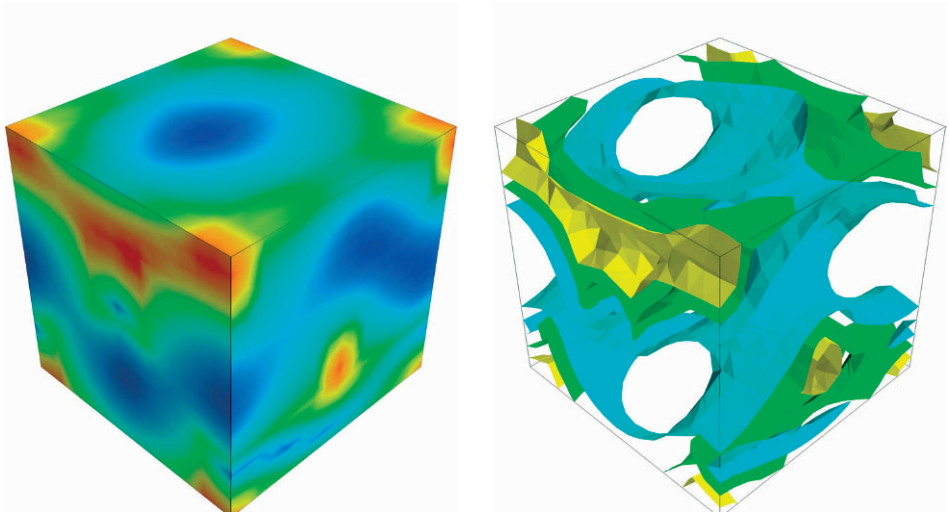

Figure 2.4: Illustration of the eigenfunction $\boldsymbol{u}^5_{h,\boldsymbol{k}}$. On the left, a surface plot of the amplitude of $|\boldsymbol{u}^5_{h,\boldsymbol{k}}|$ and on the right isosurfaces are displayed.

[25] A. V. Knyazev and K. Neymeyr. A geometric theory for preconditioned inverse iteration. III: A short and sharp convergence estimate for generalized eigenvalue problems. *Linear Algebra and its Applications*, 358(1):95–114, 2003.

[26] P. Monk. *Finite Element Methods for Maxwell's Equations*. Clarendon Press, Oxford, 2003.

[27] J. Schöberl. Commuting quasi interpolation operators for mixed finite elements, 2002. Report ISC-01-10-MATH, Texas A&M.

[28] C. Wieners. Distributed point objects. A new concept for parallel finite elements. In R. Kornhuber, R. Hoppe, J. Priaux, O. Pironneau, O. Widlund, and J. Xu, editors, *Domain Decomposition Methods in Science and Engineering*, volume 40 of *Lecture Notes in Computational Science and Engineering*, pages 175–183. Springer, 2004.

[29] C. Wieners. A geometric data structure for parallel finite elements and the application to multigrid methods with block smoothing. *Computing and Visualization in Science*, 13:161–175, 2010.

[30] S. Zaglmayr. *High order finite element methods for electromagnetic field computation*. PhD thesis, Johannes Kepler Universität Linz, 2006.

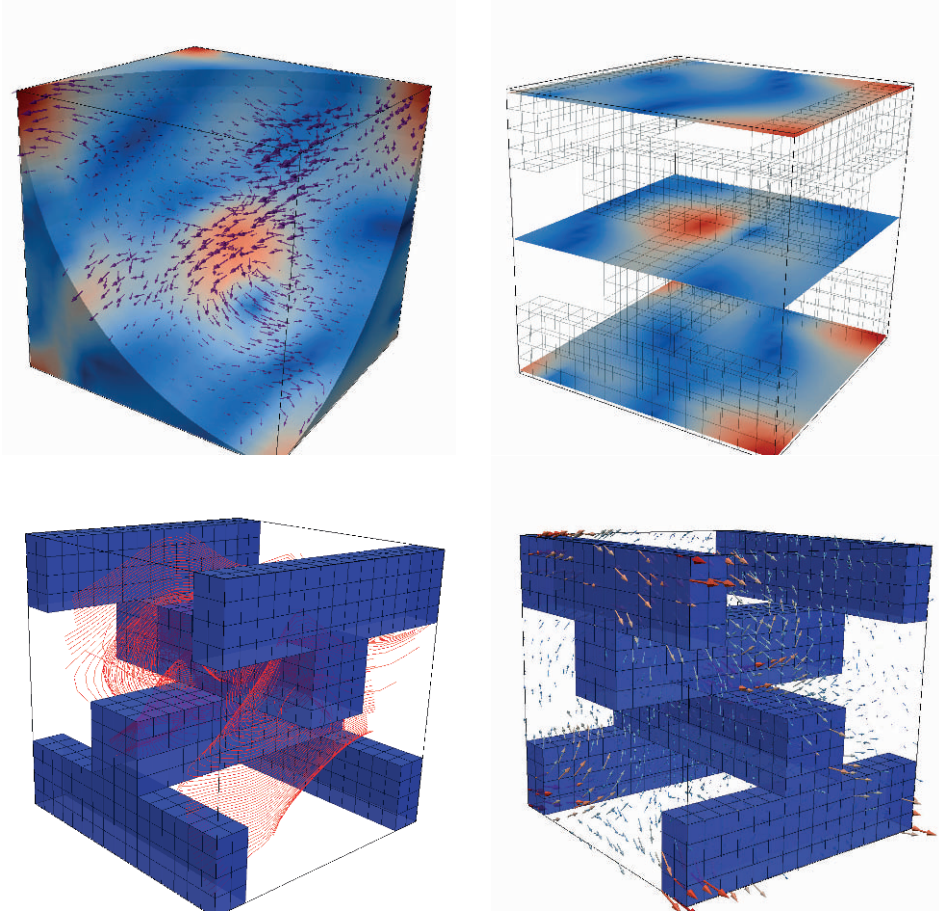

Figure 2.5: Illustration of the eigenfunction $\boldsymbol{u}^6_{h,\boldsymbol{k}}$ for $\boldsymbol{k} = (3, 1, -2)$. The cutting planes (top row) show the amplitude of the magnetic energy distribution $|\boldsymbol{u}^6_{h,\boldsymbol{k}}|$, the streamlines and the arrow-plot (bottom row) represent the vector field $\boldsymbol{u}^6_{h,\boldsymbol{k}}$.

http://www.springer.com/978-3-0348-0112-6

Photonic Crystals: Mathematical Analysis and Numerical Approximation

Dörfler, W.; Lechleiter, A.; Plum, M.; Schneider, G.; Wieners, C.

2011, VIII, 162 p., Softcover
ISBN: 978-3-0348-0112-6
A product of Birkhäuser Basel